ACSNANO
www.acsnano.org
ARTICLE

Vertical 2D/3D Semiconductor Heterostructures Based on Epitaxial Molybdenum Disulfide and Gallium Nitride

Dmitry Ruzmetov,*[,†,§] Kehao Zhang,[‡] Gheorghe Stan,[§] Berc Kalanyan,[§] Ganesh R. Bhimanapati,[‡] Sarah M. Eichfeld,[‡] Robert A. Burke,[†] Pankaj B. Shah,[†] Terrance P. O'Regan,[†] Frank J. Crowne,[†] A. Glen Birdwell,[†] Joshua A. Robinson,[‡] Albert V. Davydov,[§] and Tony G. Ivanov*[,†]

[†]Sensors and Electron Devices Directorate, U.S. Army Research Laboratory, Adelphi, Maryland 20783, United States

[‡]Department of Materials Science and Engineering & Center for Two-Dimensional and Layered Materials, The Pennsylvania State University, University Park, Pennsylvania 16802, United States

[§]Material Measurement Laboratory, National Institute of Standards and Technology, Gaithersburg, Maryland 20899, United States

Supporting Information

ABSTRACT: When designing semiconductor heterostructures, it is expected that epitaxial alignment will facilitate low-defect interfaces and efficient vertical transport. Here, we report lattice-matched epitaxial growth of molybdenum disulfide (MoS_2) directly on gallium nitride (GaN), resulting in high-quality, unstrained, single-layer MoS_2 with strict registry to the GaN lattice. These results present a promising path toward the implementation of high-performance electronic devices based on 2D/3D vertical heterostructures, where each of the 3D and 2D semiconductors is both a template for subsequent epitaxial growth and an active component of the device. The MoS_2 monolayer triangles average 1 μm along each side, with monolayer blankets (merged triangles) exhibiting properties similar to that of single-crystal MoS_2 sheets. Photoluminescence, Raman, atomic force microscopy, and X-ray photoelectron spectroscopy analyses identified monolayer MoS_2 with a prominent 20-fold enhancement of photoluminescence in the center regions of larger triangles. The MoS_2/GaN structures are shown to electrically conduct in the out-of-plane direction, confirming the potential of directly synthesized 2D/3D semiconductor heterostructures for vertical current flow. Finally, we estimate a MoS_2/GaN contact resistivity to be less than 4 $\Omega\cdot cm^2$ and current spreading in the MoS_2 monolayer of approximately 1 μm in diameter.

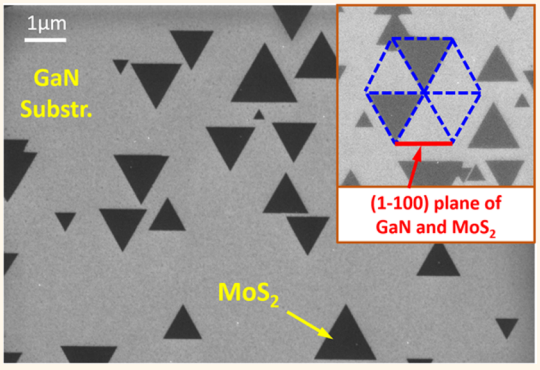

KEYWORDS: *2D material heterostructures, transition metal dichalcogenides, MoS_2, van der Waals epitaxy, GaN, conductive atomic force microscopy, vertical transport*

Two-dimensional semiconducting transition metal dichalcogenides (TMDs) are promising candidates for high-performance electronic and optoelectronic devices because they exhibit atomically sharp interfaces, ultrathin dimensions, flexibility, and large optical effects.[1−3] For example, MoS_2 is one of the most studied 2D TMDs and has been tested in proof-of-concept ultrafast field-effect transistors (FETs), optical devices, and flexible electronics.[4−9] In general, however, the highest mobility 2D MoS_2 is obtained by exfoliation of geological MoS_2 crystals and mechanically transferred to the desired substrate. Small specimen sizes, uncertainty in placement location, and lack of control over the MoS_2 crystal composition are the main drawbacks to using the geological material source.[5,10] Attempting to overcome these limitations, many have used synthetic materials to grow 2D semiconductors with engineered composition. MoS_2 has been synthesized by chemical vapor deposition (CVD),[11] metal-organic chemical vapor deposition (MOCVD),[12] and pulsed laser deposition (PLD)[13] but primarily on insulating oxide substrates. Monolayer MoS_2 has been synthesized by MOCVD on oxides, but it generally results in crystals that lack alignment, resulting in grain boundaries when crystals merge.[12] While monolayer MoS_2 has been grown partially aligned to a sapphire substrate using CVD,[11] 2D semiconductors grown on insulating substrates are limited to simple device architectures and

Received: December 18, 2015
Accepted: February 11, 2016
Published: February 11, 2016

DOI: 10.1021/acsnano.5b08008
ACS Nano 2016, 10, 3580−3588

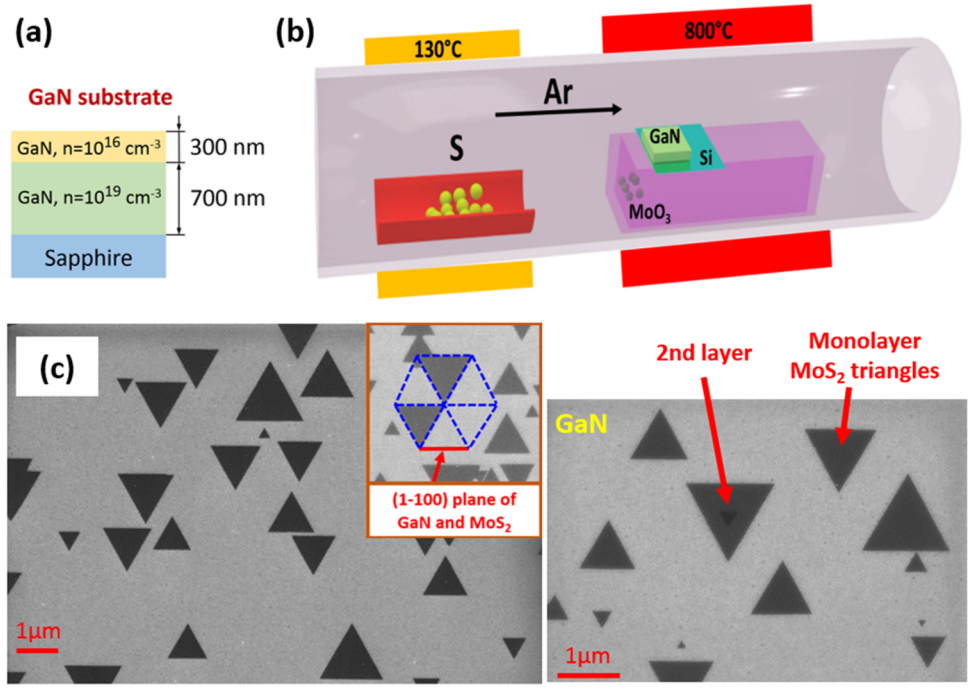

Figure 1. (a) Structure of the MOCVD GaN stack on sapphire. (b) CVD system for MoS_2 growth. (c) SEM of MoS_2 monolayer triangles on GaN epitaxial crystal. The scale bar is 1 μm and is aligned with the (1100) plane of GaN. (Inset) Orientation of the (1100) plane of hexagonal crystals of GaN and MoS_2 is shown.

generally require transfer to other substrates in order to be integrated into heterostructure devices.

On the other hand, 2D semiconductors grown with epitaxial alignment to a conventional 3D semiconductor substrate are of interest for use in hybrid 2D/3D electronic devices that employ the advantages of both the established 3D semiconductors and the unique properties of ultrathin 2D crystals.[14,15] In particular, we envision that a vertical 3D/2D/3D structure could enable high-frequency, high-power heterojunction bipolar transistor (HBT) devices, where the atomically thin 2D TMD base provides for high-speed operation and the vertical nature of the electronic transport allows for large surface area and thus high current. The utilization of MoS_2 and GaN demonstrates an example of a 2D/3D combination matching the general requirements for the vertical HBT. These requirements include close lattice match and favorable electronic band structure alignment. In addition, there is evidence that MoS_2 can serve as a growth template for GaN,[16] which gives a potential pathway to produce the top 3D component in a GaN/MoS_2/GaN stack. As an initial step toward the implementation of three- and two-terminal bipolar 2D/3D heterostructures, we investigate simple unipolar 2D/3D stacks to address the basic questions regarding the feasibility of epitaxial growth and vertical electron transport across the van der Waals gap.

In this paper, we present 2D/3D heterostructures based on the epitaxially grown MoS_2 on GaN substrates and demonstrate vertical electrical conduction across the interface. Our GaN/MoS_2 heterostructures are a lattice-matched system, unlike most reported epitaxial 2D/2D and 2D/3D heterostructures to date.[11,17,18] The MoS_2 monolayer coverage is nearly 50%, with monolayer triangles typically 1 μm along each side and monolayer blankets of up to 30 μm across. Photoluminescence and Raman microanalyses were employed to characterize monolayer MoS_2 and its interaction with the substrate. The analysis suggests that our CVD growth of epitaxial MoS_2 on GaN produces monolayer MoS_2 islands with structural quality superior to that of the mechanically exfoliated MoS_2 available to us for this study. Finally, we use conductive AFM (CAFM) to electrically characterize as-grown MoS_2/GaN heterostructures. It is important to note that using CAFM allows us to avoid processing the MoS_2/GaN heterostructure with microfabrication chemicals such as solvents and polymer resists. We demonstrate out-of-plane electrical conduction and estimate contact resistivity between the MoS_2 and GaN as well as current spreading in the MoS_2 monolayer.

RESULTS AND DISCUSSION

Epitaxial alignment between MoS_2 and GaN is predicted to exist because both GaN and MoS_2 belong to a hexagonal crystal system with in-plane lattice mismatch of <1% (GaN = 3.19 Å, MoS_2 = 3.16 Å).[19] We also expect the small discrepancy in the coefficients of thermal expansion between GaN and MoS_2 to allow the epitaxial alignment to remain when the stack is cooled from the growth temperature of MoS_2 to room temperature.[20,21] We note that quasi-epitaxial multilayer and monolayer MoS_2 films on GaN were grown by PLD.[13] Deposition of semiconductors by PLD is a straightforward method to deposit material from the target to the substrate with high deposition rates. However, PLD has inherent compositional nonuniformity issues that set limits for achieving low-defect epitaxial interfaces that are required to provide efficient carrier transport in vertical high-performance devices.

In this work, we investigate MoS_2/GaN hybrid structures on sapphire (*c*-plane) substrates. A stack of two GaN layers was grown on sapphire using MOCVD by NTT Advanced Technology Corp.: GaN (*c*-plane, Si-doped, free electron density $n = 1 \times 10^{16}$ cm^{-3}, 300 nm, top layer)/GaN (*c*-plane, Si-doped, $n = 1 \times 10^{19}$ cm^{-3}, 700 nm)//sapphire (Figure 1a). We grow MoS_2 in a CVD system using powder vaporization[22] (Figure 1b). Our CVD process is described in the Methods

DOI: 10.1021/acsnano.5b08008
ACS Nano 2016, 10, 3580−3588

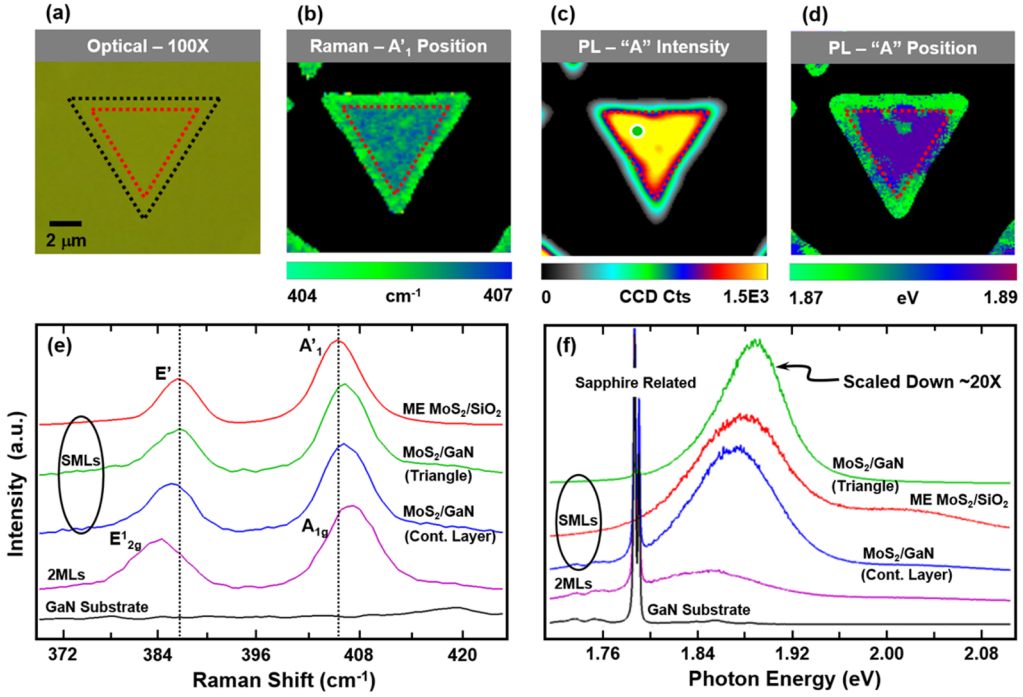

Figure 2. (a) Optical micrograph, (b) Raman image of the A′$_1$ mode peak position, (c) PL image of the intensity of the A-exciton peak, and (d) PL image of the position of the A-exciton peak. The black-dashed triangle specifies the extent of the MoS_2 growth, and the red-dashed triangle indicates the region of enhanced PL signal. (e) Raman spectra for mechanically exfoliated (ME) ML MoS_2/SiO_2, ML MoS_2/GaN isolated triangle, ML MoS_2/GaN continuous layers, two monolayers (2MLs) of MoS_2/GaN, and bare GaN substrate. Vertical dashed lines indicating the peak positons for the ME reference are added as a guide for the eyes. (f) PL spectra taken at the same data collection points as for the Raman spectra.

section and Supporting Information. Briefly, molybdenum trioxide (MoO_3) is placed in the center of a single zone furnace, and sulfur powder is placed ∼12 in. upstream of the MoO_3 crucible. The growth occurs in ultrapure argon at 800 °C for 15 min, with the sulfur heated separately by a heat tape at 130 °C. Subsequently, MoS_2 domains were characterized by scanning electron microscopy (SEM) (Figure 1c) and found to be in the form of monolayer equilateral triangles. A typical triangle size is 1 μm with some isolated triangles of up to 10 μm in size. Coalesced monolayer islands extend up to 30 μm, with no evidence of stitches when observed by SEM and AFM. There is also some trilayer and higher-order growth together with scattered 3D crystals. The striking feature is the oriented growth of the triangles (Figure 1c), where nearly all MoS_2 triangles are aligned with the rotational symmetry of the $P6_3mc$ space group of GaN.

The *c*-plane orientation of the wurtzite lattice (hexagonal crystal system) of GaN was confirmed with electron backscatter diffraction (EBSD) analysis. The *m*-plane ($1\bar{1}00$) orientation of GaN in Figure 1c (inset) was determined by EBSD to be parallel to the horizontal axis and the scale bar. The fact that the sides of triangles of MoS_2 in Figure 1c are aligned with the *m*-plane of GaN confirms the epitaxial alignment of GaN and MoS_2 lattices. Interestingly, the large monolayer islands (>10 μm in size) and triangles can be misaligned even though they also exhibit sharp, straight edges and 60° corners. At the same time, larger triangles of up to 8 μm that are oriented to the GaN are also observed. It is plausible that the initial growth that leads to larger structures originates on defects or 3D crystals (often found in the center of large MoS_2 monolayer islands) and does not occur in an epitaxial manner. The structures that nucleate later on smaller defects or no defects progress in an epitaxial manner and are smaller in size due to shorter growth time. It is also possible that epitaxial growth happens at a slower rate than misoriented growth. SEM and atomic force microscopy (AFM) do not show any stitches or flake overlaps where expanding triangles merge to form larger-area monolayers, but high-resolution microscopy would be needed to resolve the grain boundaries if any. The merging of neighboring MoS_2 triangles without grain boundaries is a prerequisite for the large-area epitaxial growth and is a vital step for the development of the field of 2D electronics.

The composition of the 2D structures, layer count, and the effect of the GaN lattice on the quality of monolayer (ML) MoS_2 were studied with Raman and photoluminescence (PL) microspectroscopies. Raman and PL hyperspectral images generated by mapping on fundamental spectral features (*e.g.*, peak position) provide useful information over several micrometer square regions with a lateral resolution on the order of the spot size of the laser (∼340 nm in our case). Regions of interest can be readily identified and explored in more detail *via* single-point measurements with increased integration times in order to bring out subtle details in the spectra. Figure 2a–d displays optical, Raman, and PL images obtained from a region where large isolated monolayer domains (∼8 μm on the side) were observed. Each domain investigated exhibits a growth direction comparable to those observed for the smaller triangles that are known to have an epitaxial relationship with the GaN substrate. The monolayer is difficult to observe in the optical image due to the absence of interference enhancement, often used with SiO_2/Si substrates for monolayer identification. To guide the reader, the domain centered in Figure 2a is outlined by a black-dashed triangle. The red-dashed triangle is the region of enhanced MoS_2/GaN

DOI: 10.1021/acsnano.5b08008
ACS Nano 2016, 10, 3580–3588

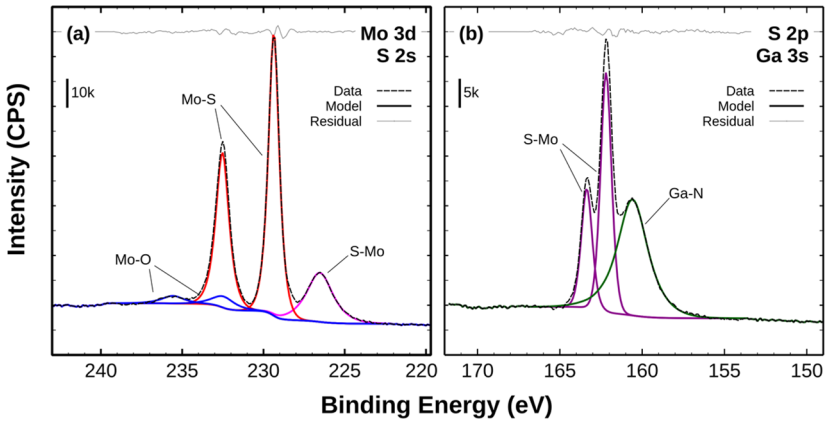

Figure 3. Core level XPS spectra and peak fits from (a) Mo 3d and (b) S 2p regions of MoS_2 on GaN. (a) Components from S 2s (MoS_2) and Mo $3d_{5/2}$ and $3d_{3/2}$ doublets (MoS_2 and MoO_x). (b) S 2p doublet (MoS_2) and Ga 3s (GaN) are shown.

lattice interaction discussed below. The material identification and monolayer character of MoS_2 are ascertained by the E′ and A'_1 Raman peak frequency difference of <20 cm^{-1} and the strength and position of the observed PL peak (Figure 2e,f and Supporting Information).

The interface-sensing spectral information on the isolated triangles and their connection to light emission properties are quite interesting. We illustrate this connection by showing what can be obtained from the hyperspectral images and then focusing our attention on single spectra taken in the regions of interest revealed by imaging. Figure 2b provides a map of the position of the out-of-plane A'_1 peak position that reveals a blue shift of the A'_1 peak in a region located away from the edge of the triangle (*i.e.*, away from the region of near-edge particles similar to those identified in Figure S7). Next, as shown in Figure 2c, this region corresponds to an area of enhanced PL signal with a rapid increase starting at ∼1 μm from the triangle's edge. As a final point to be gleaned from the images, Figure 2d reveals that this same region also maps to that of the greatest emitted photon energy.

We now turn our attention to features in the single spectra that help us interpret the observations made available by Raman and PL images. First, the Raman spectra over a wavenumber region encompassing the in-plane and out-of-plane modes are shown in Figure 2e. The spectra were obtained at points indicated in the PL images (see Figure 2c and Figure S3c in the Supporting Information) and are distinguished by the same color as the white outline circles. Additionally, results for a mechanically exfoliated (ME) ML MoS_2[23] are represented by the red curve and provide a useful reference. Most notable is the comparison between the ME reference and the MoS_2/GaN triangle. There are three main points to be made: (i) the frequency difference between the E′ and A'_1 modes of <20 cm^{-1} is consistent with ME monolayers;[24,25] (ii) peak positions for the stress-sensitive in-plane mode E′ are virtually the same, indicating stress-free (*i.e.*, relaxed) layer growth of the MoS_2/GaN (again, this holds for areas ∼1 μm distant from the triangle's edge); and (iii) as discussed in ref26, the ∼1 cm^{-1} blue shift of the A'_1 peak together with no observable change in the position of E′ is suggestive of a strengthening van der Waals contact with the adjacent GaN substrate in this region of the triangle.[26] Continuing with the remaining spectra in Figure 2e, the slight red shift of the E′ mode observed on the MoS_2/GaN continuous monolayer (ML) is consistent with a similar red shift observed at the edge of the triangle (single spectra not shown) and the expected increase in the degree of edge effects in this region. Moreover, the spectra for the two monolayer (2ML) region aligns well with that observed for similar structures in the literature.[24,25] That is, a red shift of the $^1E_{2g}$ mode and a blue shift of the A_{1g} mode result in a frequency difference of 22.6 cm^{-1}.

Figure 2f provides the PL spectra in the vicinity of the A-exciton. The data collection points on the sample and the ME MoS_2/SiO_2 reference are the same as the Raman spectra. Most remarkable is the very large (∼20×) enhancement of the PL signal obtained from the triangle as compared to ME MoS_2/SiO_2 and even the continuous ML regions of the MoS_2/GaN. This enhancement may be related to a substrate charge transfer effect,[27] stoichiometry variations,[28,29] or another unknown mechanism and will be the subject of further investigations. In addition, we see evidence of relaxed layer growth in the PL spectra. When comparing ME MoS_2, our material has a narrower PL line width and approximately the same emitted photon peak position. The smaller line width (FWHM) suggests a reduction in the lower-energy charged exciton (*i.e.*, trion) component[30] and/or an improvement in structural quality. Next, it has been shown that relaxed ME MoS_2 monolayers have a PL peak position at higher energies relative to the peak position of CVD MoS_2 on an oxide that is under tensile strain.[31] The A-exciton energy for our material is near and even at slightly higher energies than that of ME MoS_2. These observations suggest relaxed growth of our MoS_2 monolayers 1 μm away from the edges of the large triangles. Interestingly, the mentioned strain in CVD-grown materials is often acquired during the cooldown from growth temperature due to the thermal expansion coefficient mismatch with the substrate. In contrast, for our CVD growth of MoS_2 on GaN, we have a match of the thermal expansion coefficients as well as a very close match of lattice constants that likely explains the relaxed (unstrained) state of our MoS_2 on GaN. Continuing with the remaining spectra in Figure 2f, the reduction of intensity and red shift of the continuous ML of MoS_2/GaN may be understood by considering the increase in the degree of edge effects as the size of the triangles are reduced and their relative numbers enlarged. All pertinent Raman and PL spectral parameters are summarized in the Supporting Information in Tables S1 and S2, respectively. Taken as a whole, the Raman and PL analysis suggests that superior material quality can be achieved by direct growth of MoS_2 on GaN compared to the ME MoS_2 available to us for this study.

DOI: 10.1021/acsnano.5b08008
ACS Nano 2016, 10, 3580−3588

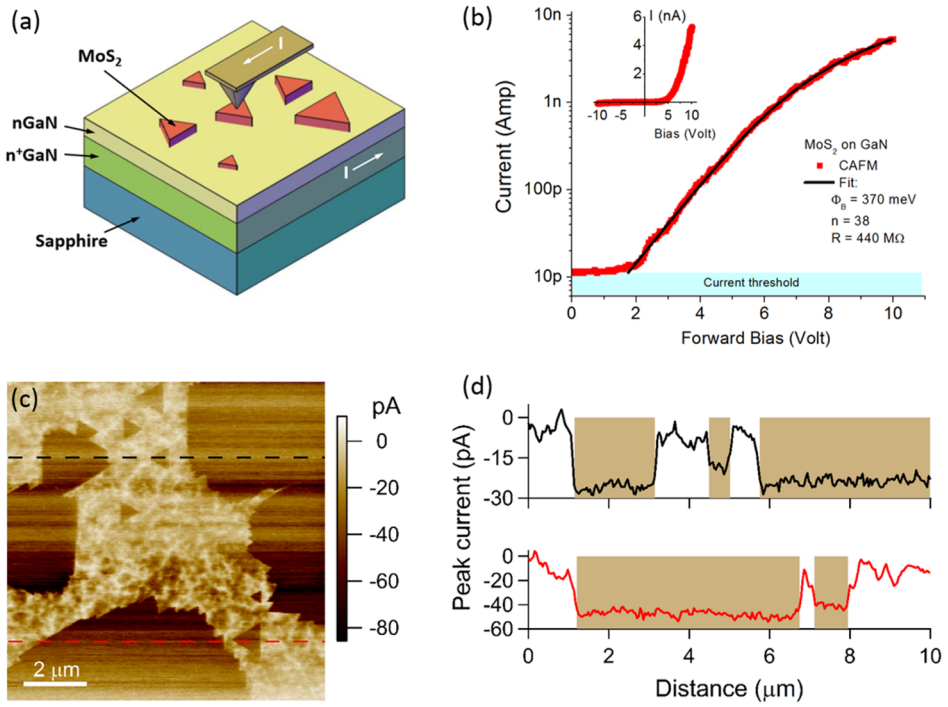

Figure 4. CAFM of MoS_2 on GaN. (a) Diagram of the measurement. (b) Forward bias $I-V$ curve on a MoS_2 monolayer. The fitting is described in Supporting Information. (Inset) Full $I-V$ curve on a linear scale for MoS_2. (c) Current map showing MoS_2 monolayer triangles. (d) Line profiles across isolated triangles and large MoS_2 areas shown in (c). The shaded areas in (d) are monolayer MoS_2.

X-ray photoelectron spectroscopy (XPS) analysis was employed to determine the composition of the 2D structures and to examine possible modifications of the GaN surface as a result of the CVD process. Figure 3 shows XPS spectra for the Mo 3d, S 2s, S 2p, and Ga 3s core levels from a MoS_2 on a GaN sample. The deconvolution of the Mo 3d region reveals Mo $3d_{5/2}$ and $3d_{3/2}$ doublets corresponding to MoS_2 (229.4 and 232.5 eV) and a weak MoO_x doublet (232.4 and 235.6 eV) related to overdeposition of MoO_x during the MoO_3 vaporization. The comparison of the areas of the S 2s and Mo 3d peaks shown in Figure 3a provides an estimate of the S/Mo ratio of 2.05 ± 0.1, consistent with stoichiometric MoS_2. The S 2s peak appears at 226.5 eV, which is characteristic of MoS_2.[32] Similarly, the S 2p doublet ($\Delta \approx 1.18$ eV) in Figure 3b is consistent with MoS_2. Thus, the XPS analysis corroborates the MoS_2 composition of the structures on the GaN substrate.

We observe an interesting feature in the topographic and adhesion maps of the MoS_2 structures (see Figure S7). There is enhanced density of topographic spikes near the edges of the triangles, and there is lower density on the bare GaN and inside the MoS_2 triangles. The origin of this particle crowding is unclear but has been studied by other research groups.[33] The reported increased oxygen content in the particles suggests that they are phases of MoO_x. As mentioned earlier, the presence of MoO_x was detected in our XPS measurements. It is possible that the redeposition of the MoO_x phase from the MoO_3 precursor happens more frequently at the edges of the triangles since the edges offer more defects that may serve as nucleation sites. This particle crowding phenomenon could potentially limit the growth of large-area MoS_2 structures when the density of the particles is high enough to disturb the growth. Other methods of the TMD growth with a better controlled environment that excludes oxygen may be required for large-area MoS_2 growth on GaN.

We investigated using XPS and an additional CVD growth whether the GaN surface is modified (*i.e.* sulfurized) during the CVD growth of MoS_2. A regular GaN/GaN//sapphire wafer (sample ID = GaN-S from here on) was run through the CVD process that was used to grow MoS_2 with the exception that the MoO_3 precursor was not introduced into the CVD tube. The GaN-S sample was exposed to the same sulfur flow in the CVD tube and at the same substrate temperature and duration as the samples with MoS_2 structures. The XPS of the GaN-S sample revealed only a weak S 2s peak at BE = 226.4 eV, which corresponds to 1.3 ± 0.1 atom % of sulfur on the surface. The spectral peak parameters of the Ga 2p, 3s and 3d peaks are not modified for the pristine GaN wafer and GaN-S sample (Figure S9c,f,g). Furthermore, the presence of the sulfur shoulder S 2p is not detectable on the Ga 3s peak (Figure S9f). We conclude that our GaN substrates are chemically stable in the CVD process. Further characterization of the sample using XPS is discussed in the Supporting Information.

We further probe the MoS_2/GaN ($n = 10^{16}$ cm^{-3}, 300 nm) heterojunction using conductive AFM (CAFM) to measure vertical charge transport. The degenerate n^+GaN ($n = 10^{19}$ cm^{-3}, 700 nm) layer served as the bottom electrode for the measurement with the AFM tip being the top nanocontact, as shown in Figure 4a. The CAFM measurements demonstrate that the MoS_2/GaN structures electrically conduct in the out-of-plane direction and across the van der Waals gap, with typical $I-V$ characteristics shown in Figure 4b. The conduction in the direction perpendicular to the sample plane opens up the possibility to combine 2D and 3D semiconductors in a vertical stack to create complex heterostructures with desired properties. For example, the crystalline order and epitaxy of our MoS_2/GaN stack should allow use of the top MoS_2 as a template for the consecutive epitaxial growth of next 2D or 3D layer to build a three-terminal device.

DOI: 10.1021/acsnano.5b08008
ACS Nano 2016, 10, 3580–3588

The results of CAFM local current maps are displayed in Figure 4c and also Figure S4b (Supporting Information). The CAFM shows enhancement of the electrical conductance on the MoS_2 monolayers *versus* the bare GaN substrate and is also observed in the current line scans in Figure 4d. One of the questions that we address in the CAFM study is how the current flows in the MoS_2 and across the MoS_2/GaN interface. If the sheet resistance of MoS_2 (R_{sh}) is considerably smaller than the contact resistance of the MoS_2/GaN interface over the area projected by the tip, $R_{sh} < \rho_c/A_{tip}$, then the current is expected to spread in the MoS_2 layer to minimize the contact resistance, $R_c = \rho_c/A_c$, where ρ_c is the MoS_2/GaN contact resistivity, A_{tip} is the CAFM tip contact area, and $A_c = \pi d_c^2/4$ is the effective contact area of MoS_2/GaN with the characteristic contact size d_c (which is roughly the contact transfer length commonly used to treat metal–semiconductor contacts). In this case, the CAFM conductivity in the current maps should be uniform across the MoS_2 layer within the distance d_c. If the opposite is true, $R_{sh} > \rho_c/A_{tip}$, then the current will travel vertically and will vary across the MoS_2 surface on the length scale $\sqrt{A_{tip}}$. The CAFM current maps over the MoS_2 triangles in Figure 4c and Figure S4b show that the enhanced current level on the MoS_2 triangles and monolayer blankets is stable over the 1 μm size areas compared to relatively large current fluctuations on the GaN substrate with the GaN feature sizes under 100 nm. This is indicative of large MoS_2/GaN contact areas ($d_c \geq 1$ μm) and considerably smaller GaN/n^+GaN contact area and resistivity. In order to estimate d_c, the CAFM area maps were measured over large MoS_2 monolayers and small triangles (Figure 4c). In the two line scans shown in Figure 4d, the current level on the 1 μm triangles is roughly 75% of the current level on monolayer islands. The higher resistance on the triangles can be explained with lower contact area limited by the triangle size, $A_{triangle} < A_c$. Since the CAFM current level does not scale with the MoS_2 area and increases only by a fraction of the current on triangles, d_c is expected to be greater than or equal to the triangle size and can be estimated as $d_c \approx 1$ μm ($A_c \approx 1$ μm^2). Interestingly, the current spreading at the corners of the triangles is expected to be limited and is reflected in the measurement by a slightly lower current level at the left of both small triangles in the line scans in Figure 4d.

Current spectroscopy using a CAFM tip was performed at several point locations on MoS_2 monolayers and on the GaN substrate. The details of the measurements and analysis are described in the Supporting Information. For both types of point locations, on MoS_2 and GaN, the shape of CAFM current–voltage curves is mostly determined by the tip–semiconductor interface that introduces the largest resistance to the current. The contribution of the MoS_2/GaN interface and the rest of the substrate is manifested only at larger currents ($I > 0.5$ nA) as an additional Ohmic drop, $I{\cdot}R$. We find that the I–V curves can be fitted with the model of thermionic emission over the Schottky barrier between the tip and top semiconductor layer when the Ohmic drop $I{\cdot}R$ is included to account for the difference between the applied voltage and the voltage dropped across the Schottky barrier. An example of three-parameter fitting is displayed in Figure 4b. Despite the unusually large ideality factor, $n = 38$, the Schottky barrier height $\Phi_B = 370$ meV is near the value reported in the literature.[34] The extraction of the resistance $R = 440$ MΩ can be used to characterize the buried MoS_2/GaN interface, which is of primary interest for this study. Using the previously estimated MoS_2/GaN contact size, $A_c = 1$ μm^2, the contact resistivity can be evaluated to be below $\rho_c \leq RA_c = 4$ Ω cm^2. The fact that the constant resistance ($R = 440$ MΩ) fit provides an excellent match to the MoS_2 data in Figure 4b is consistent with an Ohmic MoS_2/GaN contact.

Kelvin probe force microscopy (KPFM) was employed to measure the electric surface potential of MoS_2 on GaN. The correct scale of the surface potential (SP) images was confirmed with a test scan on an Al–Si–Au calibration sample. In Figure 5, the KPFM images of MoS_2 triangles and monolayer islands displayed a clear SP contrast between MoS_2 and GaN substrates. As shown in Figure 5, we consistently measure a 360 mV SP difference between the GaN and MoS_2. The work function is evaluated first by calibrating the SP level on gold to the work function of 5.1 eV. Then we measure the work functions of MoS_2 and GaN to be 4.46 and 4.11 eV, respectively. This is consistent with the work function of the monolayer MoS_2 reported in the literature in the range from 4.0 to 5.1 eV.[3,35] We found the difference in SP between a monolayer and bilayer MoS_2 to be under 30 meV (see also Figure S7).

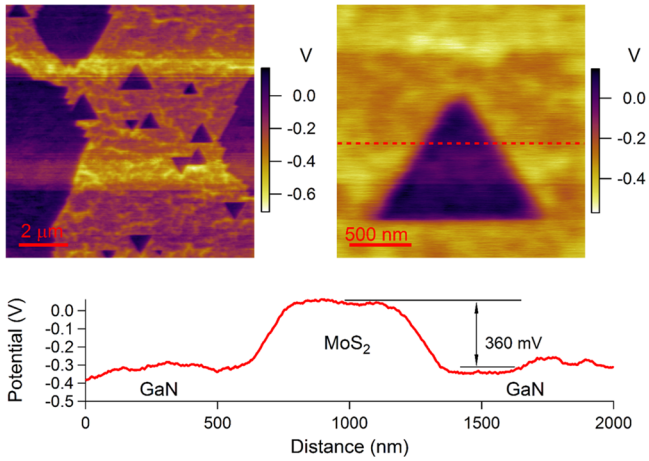

Figure 5. Kelvin probe force microscopy images showing 360 mV offset of the surface potential of MoS_2 and GaN.

The AFM topographical measurements of the MoS_2 monolayers are strongly affected by the topography of the GaN substrate that consists of a series of terrace steps (see Figures S4, S5, and S7). The step height of a single MoS_2 monolayer (7 Å) is just distinguishable from the noise. Interestingly, the second layer growth and higher-order stacking of MoS_2 monolayers can be measured reliably to be near 7 Å per monolayer due to lower noise level of the scans on MoS_2. The phase area maps of the amplitude modulation AFM images show clear contrast of the MoS_2 monolayers on the background of GaN (see Figure S5). We use the phase contrast images to simply identify the MoS_2 growth and the topography maps to readily show if the higher-order MoS_2 stacking is present (see Figure S5). Based on the contrast observed between the adhesive properties of the two materials (refer to the adhesion maps shown in Figure S7), it is likely that the phase contrast between the two materials is due to differences between their adhesive properties.

DOI: 10.1021/acsnano.5b08008
ACS Nano 2016, 10, 3580–3588

CONCLUSIONS

We grew MoS_2 monolayers epitaxially aligned to GaN substrates by means of powder vaporization. Raman spectroscopy and PL provide evidence of a high-quality van der Waals interface between the MoS_2 and GaN substrate with 20-fold photoluminescence enhancement observed in the center regions of large-area MoS_2 monolayers. Measurements with CAFM showed that the MoS_2/GaN structures electrically conduct in the out-of-plane direction and across the van der Waals gap, which opens up a possibility to combine 2D and 3D semiconductors in a vertical stack to create complex heterostructures with desired properties. The CAFM analysis suggests interface resistivity measured under 4 Ω cm^2 and an in-plane current spreading in the MoS_2 layer estimated to be approximately 1 μm in diameter. The KPFM measurements revealed a 360 mV contrast between MoS_2 and GaN surface potentials. The deduced work functions of MoS_2 and GaN were 4.46 and 4.11 eV respectively. The CAFM current spectroscopy shows that the $I-V$ curves on tip/MoS_2/GaN structures can be described with the thermionic emission model with unusually large ideality factor n = 38 and tip/MoS_2 Schottky barrier height of Φ_B = 370 meV. Epitaxial MoS_2/GaN heterostructures present a promising platform for the design of energy-efficient, high-speed, high-power vertical devices incorporating 2D-layered materials with 3D semiconductors.

METHODS

MoS_2 Growth. The MoS_2 was grown on a GaN substrate *via* a powder vaporization technique. Two milligrams of molybdenum trioxide, MoO_3 (99.8%, Sigma-Aldrich), was placed in the center of a single zone furnace, and 200 mg of sulfur powder (99.995%, Alfa Aesar) was placed ~12 in. upstream of the MoO_3 crucible. In order to eliminate the water and organic residual in the system, 10 min vacuum (0.018 Torr) annealing at 300 °C was employed before the growth. The sulfur was heated at 130 °C right after the annealing. The growth was set at 800 °C and 710 Torr for 15 min with 100 sccm ultrapure argon flow. The schematic of the full temperature ramp profile of the furnace during the growth is shown in Figure S1 in the Supporting Information.

PL and Raman Spectroscopy. The MoS_2/GaN heterostructures were characterized *via* photoluminescence and Raman spectroscopies with a WITec Alpha 300RA system using a 2.33 eV laser excitation energy. Incident laser power was adjusted in order to keep the power density at ~5.5 mW/μm^2 for single spectra data. Raman and PL images were developed over several square micrometer regions using a 250 nm grid spacing with integration times as large as 6 s. Regions of interest were identified from these maps for which single spectra were obtained using a 2 s integration time and 60 accumulations.

XPS. The composition of the MoS_2 structures and changes to the surface of the underlying GaN substrate were examined with X-ray photoelectron spectroscopy. The samples were analyzed in a Kratos Axis Ultra DLD instrument equipped with a spherical mirror analyzer. The X-rays were generated by a monochromated Al Kα source operated at 104 W. The analysis area was approximately 1 mm by 0.5 mm, and the analyzer pass energy was set to 40 eV. At least three non-overlapping spots were analyzed per sample, and the quantification results shown are the arithmetic mean of these spots. For all samples measured, a low-energy electron gun was used for charge neutralization. Despite the neutralizer, differential charging was evident between surfaces with and without MoS_2 overlayers. Using the Auger parameter 3d/$L_3M_{45}M_{45}$ for Ga (1084.05 eV), we determined that Ga is in the 3+ oxidation state for all surfaces measured.[36] In order to account for differential charging, spectra from an unprocessed GaN/GaN/sapphire surface were referenced against the hydrocarbon C 1s peak (C–H, 284.8 eV) from adventitious carbon. For this surface, the Ga $L_3M_{45}M_{45}$ Auger transition was measured at 422.6 eV. Knowing that Ga has the same oxidation state for all surfaces measured, we used the Ga $L_3M_{45}M_{45}$ Auger transition as an internal reference for the rest of the samples: MoS_2/GaN and the GaN-S sample. Peak fitting was carried out in the CasaXPS software using Gaussian–Lorentzian peak shapes and Shirley backgrounds. Relative sensitivity factors used for quantification were provided by Kratos Analytical, specifically for the Axis Ultra DLD instrument. Peaks that occurred as spin–orbit doublets were constrained to have equal FWHM values, and the expected peak area ratios for each spin state (1:2 for $p_{1/2}$ and $p_{3/2}$; 2:3 for $d_{3/2}$ and $d_{5/2}$) were also constrained.

AFM and CAFM Measurements. The (C)AFM measurements were performed on a MultiMode AFM (Bruker, Santa Barbara, California, USA) that provides nanoscale mechanical (PeakForce QNM) and electrical characterization (PeakForce Kelvin probe force microscopy (PeakForce KPFM), PeakForce tunneling atomic force microscopy (PeakForce TUNA)) in addition to common topographical imaging (amplitude modulation AFM (AM-AFM), PeakForce AFM). During mapping over selected areas, various AFM modes were used to gather a complementary characterization of the structures of interest. The MoS_2 islands were identified in the phase contrast images of AM-AFM with the AFM operated at low set-points (reduced tapping amplitudes) in which case the repulsive response from the MoS_2 increases the phase contrast of the MoS_2 islands with respect to that of the uncovered GaN regions. The enhanced dissipative response of MoS_2 in comparison with that of GaN was confirmed also in the maps of adhesive force and dissipation acquired during PeakForce AFM over areas comprising MoS_2 islands and bare GaN.

PeakForce KPFM was used to measure the surface potential of the investigated sample.[37] PeakForce KPFM is an implementation of frequency modulation KPFM on PeakForce tapping, which combines two cascaded lock-in amplifiers for the detection of the electrical gradient. The phase signal measured by the first lock-in amplifier at the resonance frequency of the cantilever is fed into the second lock-in amplifier that is locked at the KPFM modulation frequency. The output of the second lock-in amplifier is used for the KPFM feedback to cancel out the electric gradient at the modulation frequency. The PeakForce modulation was performed at 2 kHz and 50 nm amplitude, and the KPFM measurements were made during the second pass of each scanning line at 70 nm lift height. The AFM probe used for these measurements was a SCM-PIT tip (Bruker, Santa Barbara, California, USA), with the first resonance frequency at 54.1 kHz.

In PeakForce TUNA, the tip/sample current was measured during each tap of the PeakForce tapping by a linear amplifier. For these measurements, either a nitrogen-doped diamond-coated CAFM tip (NT-MDT Co.) or a conductive PtSi tip (Nanosensors, Neuchatel, Switzerland) was used, while the AFM was engaged in PeakForce tapping (30 nm tap amplitude at 1 kHz). The PeakForce TUNA was operated at −7 V dc bias and a current sensitivity of 20 nA/V.

ASSOCIATED CONTENT

Supporting Information

The Supporting Information is available free of charge on the ACS Publications website at DOI: 10.1021/acsnano.5b08008.

MoS_2 growth, Raman and photoluminescence spectroscopy, conductive atomic force microscopy study, XPS analysis (PDF)

AUTHOR INFORMATION

Corresponding Authors

*E-mail: dmitry.a.ruzmetov.ctr@mail.mil.

*E-mail: tony.g.ivanov.civ@mail.mil.

Notes

Certain commercial equipment, instruments, or materials are identified in this document. Such identification does not imply recommendation or endorsement by the National Institute of Standards and Technology nor does it imply that the products identified are necessarily the best available for the purpose.

DOI: 10.1021/acsnano.5b08008
ACS Nano 2016, 10, 3580–3588

The authors declare no competing financial interest.

ACKNOWLEDGMENTS

This work was supported by the U.S. Army Research Laboratory (ARL) Director's Strategic Initiative (DSI) program on understanding and exploiting the electronic interface in stacked 2D atomic layered materials. D.R. and A.V.D. acknowledge the support of Material Genome Initiative funding allocated to NIST. J.A.R. acknowledges support of the National Science Foundation under Grant No. DMR-1453924. The authors are grateful to Dr. Gavin Liu from NIST for performing the X-ray diffraction measurements on the GaN substrates.

REFERENCES

(1) Geim, A. K.; Grigorieva, I. V. Van Der Waals Heterostructures. *Nature* **2013**, *499*, 419−425.
(2) Jeong, H.; Bang, S.; Oh, H. M.; Jeong, H. J.; An, S.-J.; Han, G. H.; Kim, H.; Kim, K. K.; Park, J. C.; Lee, Y. H.; Lerondel, G.; Jeong, M. S. Semiconductor−Insulator−Semiconductor Diode Consisting of Monolayer MoS2, H-BN, and GaN Heterostructure. *ACS Nano* **2015**, *9*, 10032−10038.
(3) Wang, F.; Wang, Z.; Xu, K.; Wang, F.; Wang, Q.; Huang, Y.; Yin, L.; He, J. Tunable GaTe-MoS2 van Der Waals P−n Junctions with Novel Optoelectronic Performance. *Nano Lett.* **2015**, *15*, 7558−66.
(4) Krasnozhon, D.; Lembke, D.; Nyffeler, C.; Leblebici, Y.; Kis, A. MoS2 Transistors Operating at Gigahertz Frequencies. *Nano Lett.* **2014**, *14*, 5905−5911.
(5) Radisavljevic, B.; Whitwick, M. B.; Kis, A. Integrated Circuits and Logic Operations Based on Single-Layer MoS2. *ACS Nano* **2011**, *5*, 9934−9938.
(6) Radisavljevic, B.; Radenovic, A.; Brivio, J.; Giacometti, V.; Kis, A. Single-Layer MoS2 Transistors. *Nat. Nanotechnol.* **2011**, *6*, 147−150.
(7) Mak, K. F.; He, K.; Shan, J.; Heinz, T. F. Control of Valley Polarization in Monolayer MoS2 by Optical Helicity. *Nat. Nanotechnol.* **2012**, *7*, 494−498.
(8) Pu, J.; Yomogida, Y.; Liu, K.-K.; Li, L.-J.; Iwasa, Y.; Takenobu, T. Highly Flexible MoS2 Thin-Film Transistors with Ion Gel Dielectrics. *Nano Lett.* **2012**, *12*, 4013−4017.
(9) Lee, G.-H.; Yu, Y.-J.; Cui, X.; Petrone, N.; Lee, C.-H.; Choi, M. S.; Lee, D.-Y.; Lee, C.; Yoo, W. J.; Watanabe, K.; Taniguchi, T.; Nuckolls, C.; Kim, P.; Hone, J. Flexible and Transparent MoS2 Field-Effect Transistors on Hexagonal Boron Nitride-Graphene Heterostructures. *ACS Nano* **2013**, *7*, 7931−7936.
(10) Varrla, E.; Backes, C.; Paton, K. R.; Harvey, A.; Gholamvand, Z.; McCauley, J.; Coleman, J. N. Large-Scale Production of Size-Controlled MoS2 Nanosheets by Shear Exfoliation. *Chem. Mater.* **2015**, *27*, 1129−1139.
(11) Dumcenco, D.; Ovchinnikov, D.; Marinov, K.; Lazić, P.; Gibertini, M.; Marzari, N.; Sanchez, O. L.; Kung, Y.-C.; Krasnozhon, D.; Chen, M.-W.; Bertolazzi, S.; Gillet, P.; Fontcuberta i Morral, A.; Radenovic, A.; Kis, A. Large-Area Epitaxial Monolayer MoS2. *ACS Nano* **2015**, *9*, 4611−4620.
(12) Kang, K.; Xie, S.; Huang, L.; Han, Y.; Huang, P. Y.; Mak, K. F.; Kim, C.-J.; Muller, D.; Park, J. High-Mobility Three-Atom-Thick Semiconducting Films with Wafer-Scale Homogeneity. *Nature* **2015**, *520*, 656−660.
(13) Serrao, C. R.; Diamond, A. M.; Hsu, S.-L.; You, L.; Gadgil, S.; Clarkson, J.; Carraro, C.; Maboudian, R.; Hu, C.; Salahuddin, S. Highly Crystalline MoS2 Thin Films Grown by Pulsed Laser Deposition. *Appl. Phys. Lett.* **2015**, *106*, 052101.
(14) Aretouli, K. E.; Tsipas, P.; Tsoutsou, D.; Marquez-Velasco, J.; Xenogiannopoulou, E.; Giamini, S. A.; Vassalou, E.; Kelaidis, N.; Dimoulas, A. Two-Dimensional Semiconductor HfSe2 and MoSe2/HfSe2 van Der Waals Heterostructures by Molecular Beam Epitaxy. *Appl. Phys. Lett.* **2015**, *106*, 143105.
(15) Xenogiannopoulou, E.; Tsipas, P.; Aretouli, K. E.; Tsoutsou, D.; Giamini, S. A.; Bazioti, C.; Dimitrakopulos, G. P.; Komninou, P.; Brems, S.; Huyghebaert, C.; Radu, I. P.; Dimoulas, A. High-Quality, Large-Area MoSe 2 and MoSe 2/Bi 2 Se 3 Heterostructures on AlN (0001)/Si (111) Substrates by Molecular Beam Epitaxy. *Nanoscale* **2015**, *7*, 7896−7905.
(16) Gupta, P.; Rahman, A. A.; Subramanian, S.; Gupta, S.; Thamizhavel, A.; Orlova, T.; Rouvimov, S.; Vishwanath, S.; Protasenko, V.; Laskar, M. R.; Xing, H. G.; Jena, D.; Bhattacharya, A. Layered Transition Metal Dichalcogenides: Promising near-Lattice-Matched Substrates for GaN Growth. *ArXiv150908256 Cond-Mat* **2015**.
(17) Shi, Y.; Zhou, W.; Lu, A.-Y.; Fang, W.; Lee, Y.-H.; Hsu, A. L.; Kim, S. M.; Kim, K. K.; Yang, H. Y.; Li, L.-J.; Idrobo, J.-C.; Kong, J. Van Der Waals Epitaxy of MoS2 Layers Using Graphene As Growth Templates. *Nano Lett.* **2012**, *12*, 2784−2791.
(18) Okada, M.; Sawazaki, T.; Watanabe, K.; Taniguch, T.; Hibino, H.; Shinohara, H.; Kitaura, R. Direct Chemical Vapor Deposition Growth of WS2 Atomic Layers on Hexagonal Boron Nitride. *ACS Nano* **2014**, *8*, 8273−8277.
(19) Jellinek, F.; Brauer, G.; Muller, H. Molybdenum and Niobium Sulphides. *Nature* **1960**, *185*, 376−377.
(20) Huang, L. F.; Gong, P. L.; Zeng, Z. Correlation between Structure, Phonon Spectra, Thermal Expansion, and Thermomechanics of Single-Layer MoS2. *Phys. Rev. B: Condens. Matter Mater. Phys.* **2014**, *90*, 045409.
(21) Leszczynski, M.; Suski, T.; Teisseyre, H.; Perlin, P.; Grzegory, I.; Jun, J.; Porowski, S.; Moustakas, T. D. Thermal Expansion of Gallium Nitride. *J. Appl. Phys.* **1994**, *76*, 4909−4911.
(22) Zhang, K.; Feng, S.; Wang, J.; Azcatl, A.; Lu, N.; Addou, R.; Wang, N.; Zhou, C.; Lerach, J.; Bojan, V.; Kim, M. J.; Chen, L.-Q.; Wallace, R. M.; Terrones, M.; Zhu, J.; Robinson, J. A. Manganese Doping of Monolayer MoS2: The Substrate Is Critical. *Nano Lett.* **2015**, *15*, 6586−6591.
(23) Georgieva, M.; O'Regan, T. Identification and Mapping of Mechanically Exfoliated 1H-MoS2 Flakes for Field-Effect Transistors. *US Army Res. Lab.* **2014**, ARL-TR-7021.
(24) Lee, C.; Yan, H.; Brus, L. E.; Heinz, T. F.; Hone, J.; Ryu, S. Anomalous Lattice Vibrations of Single-and Few-Layer MoS2. *ACS Nano* **2010**, *4*, 2695−2700.
(25) Li, H.; Zhang, Q.; Yap, C. C. R.; Tay, B. K.; Edwin, T. H. T.; Olivier, A.; Baillargeat, D. From Bulk to Monolayer MoS2: Evolution of Raman Scattering. *Adv. Funct. Mater.* **2012**, *22*, 1385−1390.
(26) Zhou, K.-G.; Withers, F.; Cao, Y.; Hu, S.; Yu, G.; Casiraghi, C. Raman Modes of MoS2 Used as Fingerprint of van Der Waals Interactions in 2-D Crystal-Based Heterostructures. *ACS Nano* **2014**, *8*, 9914−9924.
(27) Li, Y.; Qi, Z.; Liu, M.; Wang, Y.; Cheng, X.; Zhang, G.; Sheng, L. Photoluminescence of Monolayer MoS2 on LaAlO3 and SrTiO3 Substrates. *Nanoscale* **2014**, *6*, 15248−15254.
(28) Kim, I. S.; Sangwan, V. K.; Jariwala, D.; Wood, J. D.; Park, S.; Chen, K.-S.; Shi, F.; Ruiz-Zepeda, F.; Ponce, A.; Jose-Yacaman, M.; Dravid, V. P.; Marks, T. J.; Hersam, M. C.; Lauhon, L. J. Influence of Stoichiometry on the Optical and Electrical Properties of Chemical Vapor Deposition Derived MoS2. *ACS Nano* **2014**, *8*, 10551−10558.
(29) Sangwan, V. K.; Jariwala, D.; Kim, I. S.; Chen, K.-S.; Marks, T. J.; Lauhon, L. J.; Hersam, M. C. Gate-Tunable Memristive Phenomena Mediated by Grain Boundaries in Single-Layer MoS2. *Nat. Nanotechnol.* **2015**, *10*, 403−406.
(30) Mak, K. F.; He, K.; Lee, C.; Lee, G. H.; Hone, J.; Heinz, T. F.; Shan, J. Tightly Bound Trions in Monolayer MoS2. *Nat. Mater.* **2012**, *12*, 207−211.
(31) Liu, Z.; Amani, M.; Najmaei, S.; Xu, Q.; Zou, X.; Zhou, W.; Yu, T.; Qiu, C.; Birdwell, A. G.; Crowne, F. J.; Vajtai, R.; Yakobson, B. I.; Xia, Z.; Dubey, M.; Ajayan, P. M.; Lou, J. Strain and Structure Heterogeneity in MoS2 Atomic Layers Grown by Chemical Vapour Deposition. *Nat. Commun.* **2014**, *5*, 5246.
(32) Kong, J.; Park, K. T.; Miller, A. C.; Klier, K. Molybdenum Disulfide Single Crystal (0002) Plane XPS Spectra. *Surf. Sci. Spectra* **2000**, *7*, 69−74.
(33) Ajayan, P. Oral presentation at the ARO MURI Review, 2015.

DOI: 10.1021/acsnano.5b08008
ACS Nano 2016, 10, 3580−3588

(34) Giannazzo, F.; Fisichella, G.; Piazza, A.; Agnello, S.; Roccaforte, F. Nanoscale Inhomogeneity of the Schottky Barrier and Resistivity in MoS2Multilayers. *Phys. Rev. B: Condens. Matter Mater. Phys.* **2015**, *92*, 081307.
(35) Kaushik, V.; Varandani, D.; Mehta, B. R. Nanoscale Mapping of Layer-Dependent Surface Potential and Junction Properties of CVD-Grown MoS2 Domains. *J. Phys. Chem. C* **2015**, *119*, 20136−20142.
(36) *Applications of Analytical Techniques to the Characterization of Materials*; Perry, D. L., Ed.; Springer: Boston, MA, 1991.
(37) Zerweck, U.; Loppacher, C.; Otto, T.; Grafström, S.; Eng, L. M. Accuracy and Resolution Limits of Kelvin Probe Force Microscopy. *Phys. Rev. B: Condens. Matter Mater. Phys.* **2005**, *71*, 125424.

DOI: 10.1021/acsnano.5b08008
ACS Nano 2016, 10, 3580−3588

Title: **Vertical 2D/3D Semiconductor Heterostructures Based on Epitaxial Molybdenum Disulfide and Gallium Nitride**

Authors: Dmitry Ruzmetov[1,3], Kehao Zhang[2], Gheorghe Stan[3], Berc Kalanyan[3], Ganesh R. Bhimanapati[2], Sarah M. Eichfeld[2], Robert A. Burke[1], Pankaj B. Shah[1], Terrance P. O'Regan[1], Frank J. Crowne[1], A. Glen Birdwell[1], Joshua A. Robinson[2], Albert V. Davydov[3], Tony G. Ivanov[1]

Affiliations:

1. Sensors and Electron Devices Directorate, US Army Research Laboratory, Adelphi, MD 20783, USA.

2. Department of Materials Science and Engineering & Center for Two-Dimensional and Layered Materials, The Pennsylvania State University, University Park, PA 16802, USA.

3. Material Measurement Laboratory, National Institute of Standards and Technology, Gaithersburg, MD 20899, USA.

Date: Wednesday, February 10, 2016

Supporting Information.

1. MoS_2 growth and substrate quality

The MoS_2 was grown on GaN substrate *via* powder vaporization technique. 2 mg MoO_3 (99.8%, Sigma Aldrich) is placed in the center of a single zone furnace, and 200mg sulfur powder (99.995%, Alfa Aesar) is located ~12 inch upstream of the MoO_3 crucible. Before starting growth a 10 minute vacuum (0.018 Torr) anneal at 300˚C was used to eliminate water and organic residuals in the furnace. Sulfur was heated at 130˚C immediately after the annealing. The growth temperature was then set at 800˚C and 710 Torr for 15 minutes with 100sccm ultra-pure argon flow. The schematic of the full temperature ramp profile of the furnace during the growth is shown in Figure S1.

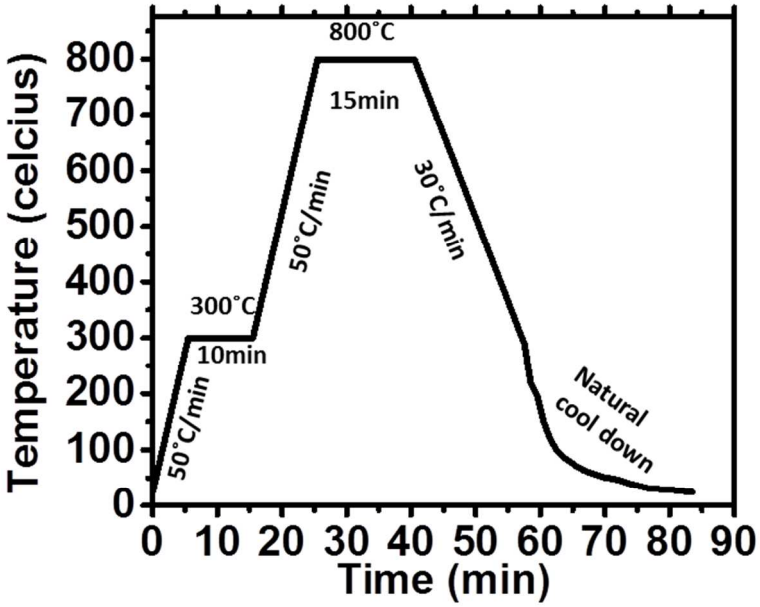

Figure S1. The temperature ramp profile of the CVD furnace during the growth of MoS_2 on GaN. The growth occurs at 800°C.

The roughness of GaN substrate has significant impact on the MoS_2 film quality. As an example, two types of GaN substrates were tested for the MoS_2 growth: a) Sapphire(c-plane)//GaN(HVPE, 5.5µm thick, free hole density p=1.2e18cm^{-3}, Mg-doped) and b) Sapphire(c-plane)//GaN(MOCVD, 700nm thick, epitaxial, free electron density n=1e19cm^{-3}, Si-doped)/GaN(MOCVD, 300nm thick, epitaxial, n=1e16cm^{-3}, Si-doped). The HVPE substrate was grown by hydride vapour phase epitaxy and the MOCVD substrate was grown by metalorganic chemical vapour deposition. The quality of the GaN substrates before the MoS_2 growth was analyzed by atomic force microscopy (AFM), see Figure S2a,b. The p-GaN substrate was measured to be significantly more rough (arithmetic average of absolute values surface roughness Ra=0.70nm) and has particles on the surface as compared to the n-GaN substrate (Ra=0.21nm). The CVD growth of MoS_2 was performed on both types of substrates using procedures similar to what we described above. The scanning electron microscopy (SEM, Figure S2c) and AFM (Figure S2e) analysis of the MoS_2 growth on the p-GaN substrate shows mostly the absence of the oriented 2D growth with characteristic thicknesses of MoS_2 structures of 5nm. At the same time, the MoS_2 grown on smooth n-GaN substrates shows epitaxial alignment and monolayer thicknesses.

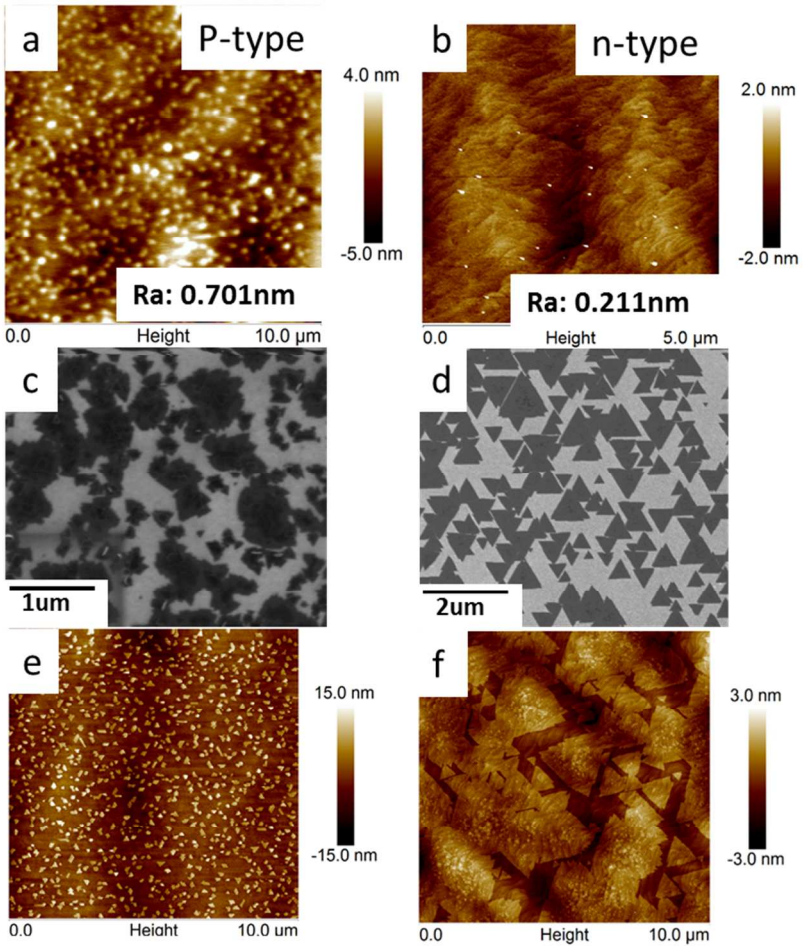

Figure S2. Comparison of the MoS_2 growth on the GaN substrates of different roughness. AFM maps of bare GaN substrates grown by (a) HVPE, p-GaN, and (b) MOCVD, n-GaN. SEM images of the resulting MoS_2 structures on (c) p-GaN and (d) n-GaN. AFM maps of MoS_2 on (e) p-GaN and (f) n-GaN.

2. Raman and Photoluminescence

Raman and photoluminescence (PL) spectroscopy has been utilized extensively to investigate MoS_2 from a few molecular layers (MLs) down to a single-molecular layer (SML)[1,2]. Here, we provide a very brief review detailing some of the information made available by these techniques.

The Raman spectra are dominated by two characteristic Raman-active modes, noted as the in-plane E^1_{2g} and the out-of-plane A_{1g} modes in few layer systems. Since there is no center of inversion for a SML of MoS_2, E' and A'_1 are used instead of the common E^1_{2g} and A_{1g} notations when reference is made to the SML in this work. One of the most distinctive properties of confining the system to fewer layers is the redshift of the A_{1g} mode and blueshift of the E^1_{2g} phonon mode with decreasing number of layers. The blueshift of the E^1_{2g} peak was shown to be due to dielectric screening of the long-range Coulomb interaction,[3] while the redshift of the A_{1g} mode is in line with the classical picture of a harmonic potential.[4] As such, the frequency difference between E^1_{2g} and A_{1g} is often used to identify the number of MoS_2 layers. These two characteristic Raman modes have phonon frequency in the SML limit of ~385 cm^{-1} and ~405 cm^{-1}, respectively.

Other perturbations can also affect the peak positions of these characteristic phonon modes, e.g., strain and doping.[5,6] Work concerning the effect of strain shows that the in-plane E^1_{2g} mode is sensitive to strain, while the out-of-plane A_{1g} mode shows a weak strain dependence.[5] These two modes show distinct doping dependence; with the A_{1g} mode decreasing in frequency with increased electron concentration, and the E^1_{2g} mode showing an overall weak dependence on electron concentration.[6] This difference is attributed to the stronger coupling to electrons of the A_{1g} mode compared with the E^1_{2g} mode. As a final point, recent work by Zhou and coworkers demonstrate that a blueshift of the A_{1g} mode is indicative of the strength of the van der Waals contact with the adjacent substrate.[7]

The conversion of an indirect gap material to one with a direct gap when the layer count is reduced to a single-molecular layer (SML) is one of the most astonishing features of many layered van der Waals materials such as MoS_2.[8,9] Reduction to a SML of MoS_2 results in considerable light emission due to direct exciton recombination at a photon energy of ~1.8-1.9 eV. This photon energy is significantly lower than the first direct gap due to the existence of a very strong binding energy of the 2D excitons as recently demonstrated by several research groups.[10–12] Two distinct peaks in the PL spectra may be observed near this energy range and are due to spin-orbit-induced splitting of the valence band. The most intense and lowest energy feature is known as the "A" exciton peak, whereas the much lower intensity and higher energy peak is the "B" exciton. The A-exciton peak is the PL feature of interest in this study. It should be noted that the intensity of A-exciton peak can be highly variable and is dependent upon the host substrate.[13] Furthermore, a considerable PL enhancement can result from physisorption of certain molecules that act as p-type dopants.[14] The energy position and width (FWHM) of this PL peak provides useful information related to the layer count, strain-state, and structural quality of the 2D layer.

Figure S3(a,b,c) displays optical, Raman, and PL images taken at a region where small triangles have merged into continuous SMLs or layer stacks of 2 or more MLs. This region is chosen to demonstrate the high selectivity of Raman and PL dependence on the layer count. Features in the Raman image (Figure S3b) are indicative of increased layer thickness with the greatest intensity originating from regions with the largest number of layers. Features in the PL image (Figure S3c) corroborate those observed with Raman with regions of no-growth (black regions), SML growth (bright regions), and 2 or more MLs (grey

regions) easily identifiable. The colored circles with white outline note points where single spectra were taken and were shown in the main text in Figure 2e,f.

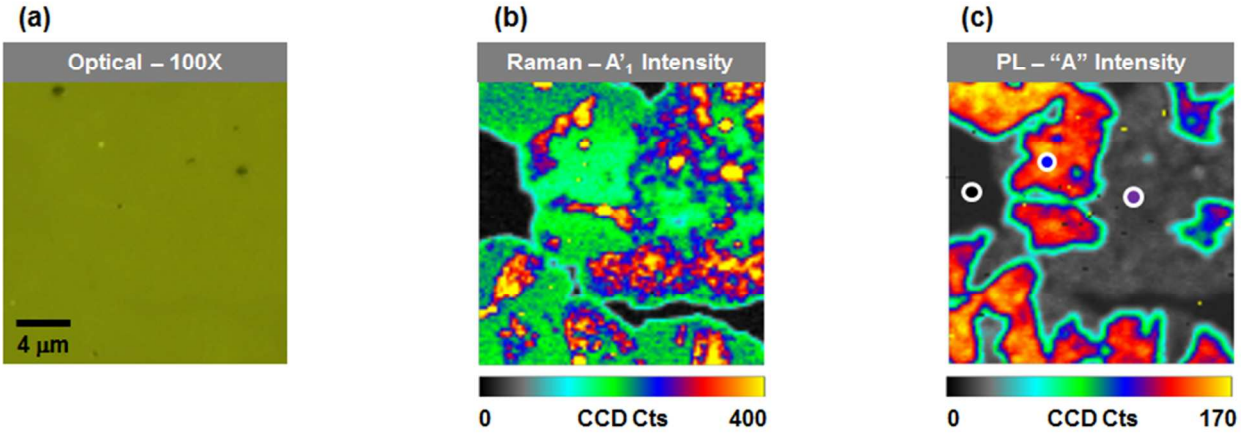

Figure S3. (a) Optical micrograph, (b) Raman image of the A'_1 mode intensity, and (c) PL image of the intensity of "A" exciton peak taken at a region where small triangles have merged into continuous SMLs or layer stacks of 2 or more MLs.

Table S1. Raman spectral parameters corresponding to spectra shown in Figure 2e in the main text.

	E' or E^1_{2g} Mode (cm^{-1})		**A'_1 or A_{1g} Mode (cm^{-1})**	
Structure	**Peak Position**	**FWHM**	**Peak Position**	**FWHM**
ME MoS_2/SiO_2	386.5	5.5	405.4	6.4
MoS_2/GaN – Large Triangle	386.5	6.6	406.3	6.5
MoS_2/GaN – Continuous SML	385.7	6.6	406.2	6.8
MoS_2/GaN – 2-Molecular Layers	384.5	7.5	407.1	7.1

Table S2. Photoluminescence spectral parameters corresponding to spectra shown in Figure 2f in the main text. The ratio of the PL intensity (I_{lum}) and Raman intensity (I_{Raman}) is used as a measure of the intrinsic luminescence quantum efficiency as describe by Splendiani and coworkers.[8]

	"A" Exciton		
Structure	**Peak Position (eV)**	**FWHM (meV)**	**I_{Lum}/I_{Raman}**
ME MoS_2/SiO_2	1.875	91	16
MoS_2/GaN – Large Triangle	1.883	63	400
MoS_2/GaN – Continuous SML	1.868	82	17
MoS_2/GaN – 2-Molecular Layers	1.845	116	3

3. Conductive atomic force microscopy study

Conductive atomic force microscopy (CAFM) as well as other types of atomic force microscopy (AFM) were used to characterize the MoS_2 structures on GaN. The details on the CAFM and AFM techniques and nano-probes (tips) used are given in the Methods section of the main text. During a CAFM measurement a CAFM tip was grounded and served as the top nano-electrode while the degenerately n-doped GaN layer on the substrate was biased and served as the bottom contact to the MoS_2/GaN stacks, as depicted in the measurement diagram in Figure 4a. Large area (A_{back}) Ti(bottom)/Au pads near the edges of the sample were evaporated on the top of the GaN wafer and served as the contacts to the bottom electrode, n^+GaN. Evaporation of the contacts with shadow masks allowed to avoid the contact of the samples with microfabrication chemicals. The Ti/Au contacts were non-ohmic but introduced only insignificant (due to large $A_{back} \gg A_c$) contact resistance ($R_{back} \propto A_{back}^{-1}$) below 1 kΩ thus contributing negligible uncertainty (< 6 μV) to the tip-to-n^+GaN bias at the currents measured.

In CAFM areal imaging, the substrate was biased at a constant voltage and the measured current was mapped. Topographical AFM imaging that included phase contrast imaging was usually performed over the area selected for the CAFM current mapping. A topographic map and corresponding current map of the MoS_2 structures on GaN substrate are displayed in Figure S4. The amplitude modulation AFM maps of the topography and phase contrast are displayed in Figure S5. Phase contrast images readily distinguish MoS_2-covered areas from GaN surface. The topographic images display a terrace-like structure of the GaN substrate with ultra-thin triangles and blankets of MoS_2 scattered on the surface. A topographic line scan across a MoS_2 triangle is shown in Figure S4 with a vertical step in the place of the triangle just standing out from the background noise and consistent with 0.7 ± 0.5 nm height. Second layer triangles and higher order growth can be readily seen in topographic AFM images (Figure S5) due to lower noise level on the MoS_2 structures and measure approximately 0.7 nm per monolayer. Areal and line CAFM scans at -7V substrate bias shown in Figure S4b display the increase of conductivity on the MoS_2 triangles and the uniform current level throughout the triangles likely due to the current spreading in the MoS_2 layer. There are obvious fluctuations in the current level outside the triangles and on the GaN substrate (Figure S4b). Secondary electron microscopy (SEM) analysis of the GaN substrate areas in between the MoS_2 triangles reveals some disordered, nanoscale growth structures in the form of clusters of nano-particles visible only at high magnification. The topographic AFM analysis shows that those nascent, disordered growth structures, if present, must be generally no more than a MoS_2 monolayer in height. The nature of the observed nanoscale growth on GaN is unclear and it may be either a sub-monolayer of MoS_2 that later develops into ML MoS_2 or another material such as MoO_x. We speculate that those current fluctuations in the CAFM areal image (Figure S4b) come from the enhancement of the conduction on nanoscale growth structures on the GaN substrate.

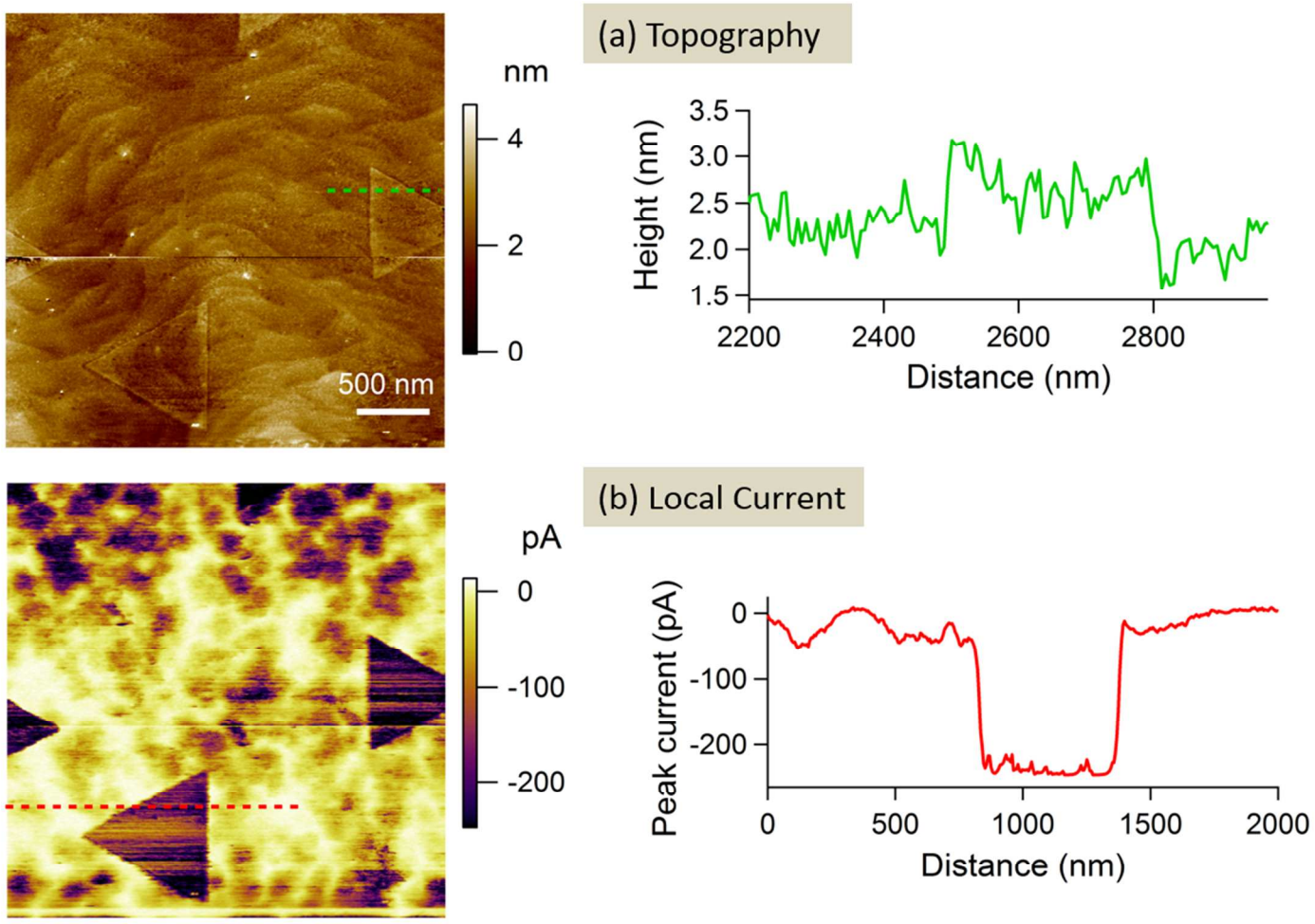

Figure S4. Conductive AFM measurements on MoS_2. (a) Topography map and a line scan (b) Local current map and a line scan across a MoS_2 triangle. The current and conductivity are enhanced on the MoS_2 monolayer triangles.

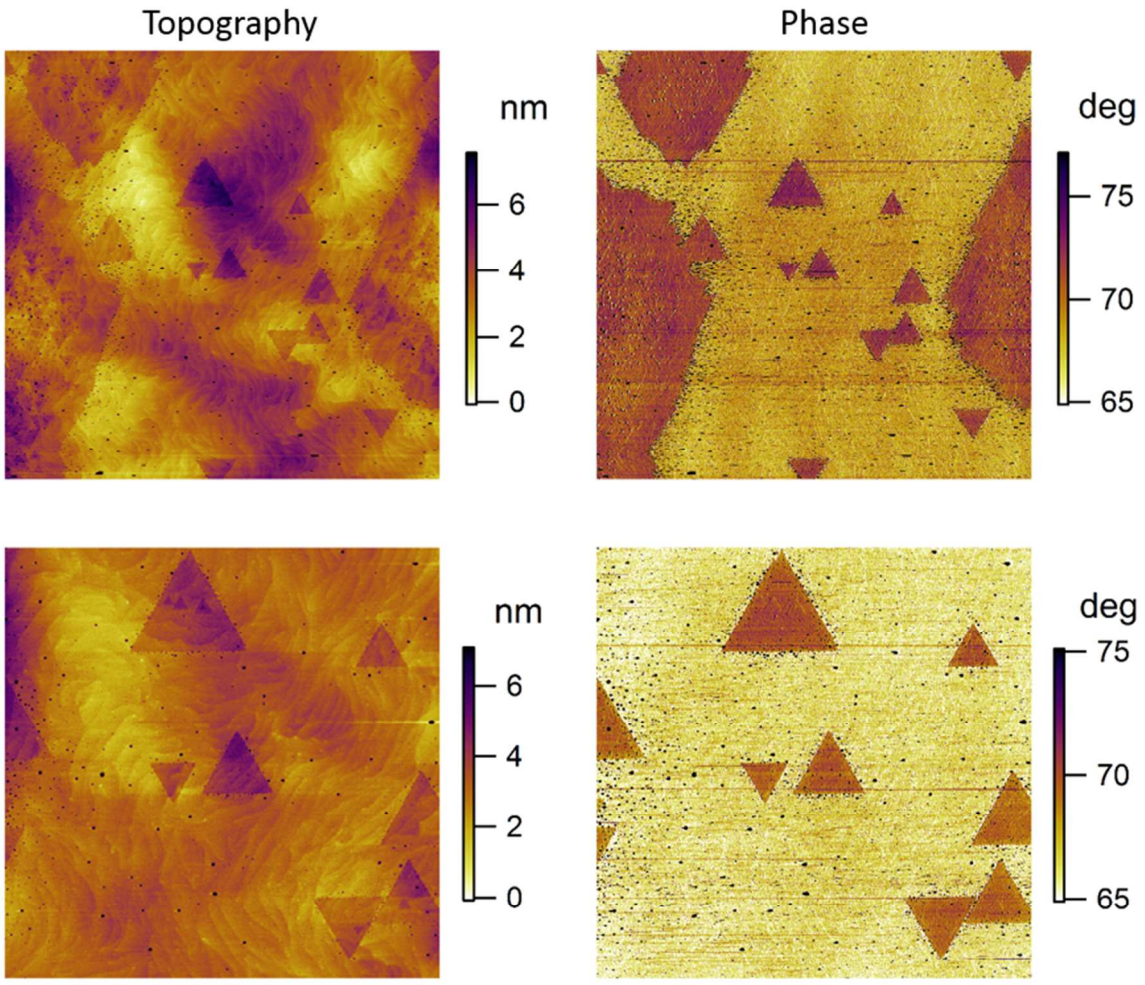

Figure S5. AFM characterization of the MoS_2 on GaN terraced surface. (Left) Topography maps point out the higher order layer count. (Right) The phase maps distinguish between MoS_2 and GaN. (Top) Map size 10um x 10um. (Bottom) 5um x 5um.

I-V spectroscopy at selected points on the sample surface was performed with the CAFM tip. Typical measured current-voltage curves for the MoS_2 monolayer and GaN substrate are displayed in Figure S6a. The voltage polarity on the graphs in Figure S6 is chosen so that the positive voltage corresponds to the forward Schottky bias, i.e. electrons are injected from the semiconductor sample to the conductive tip.

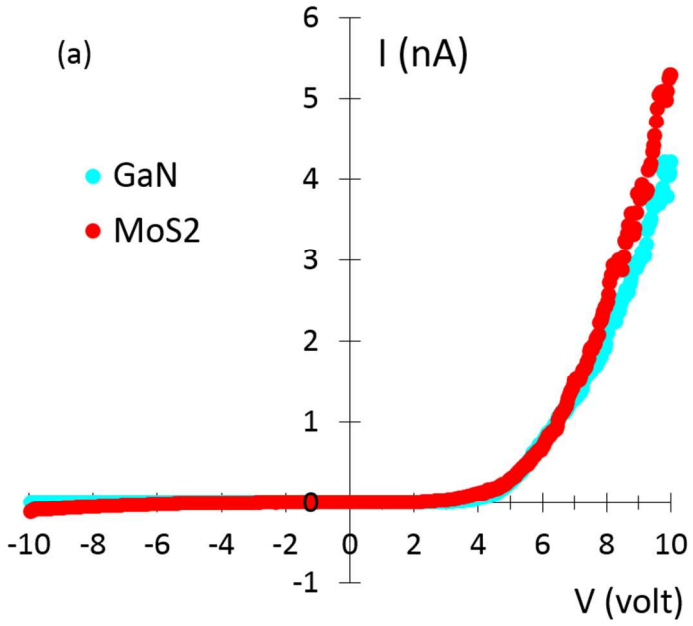

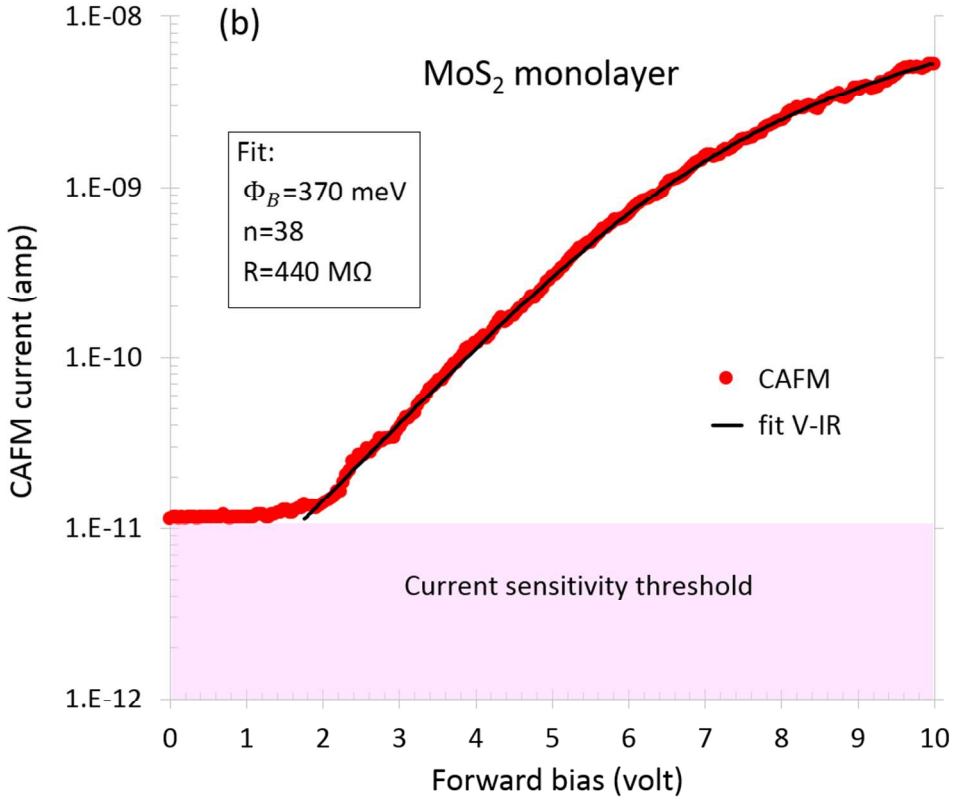

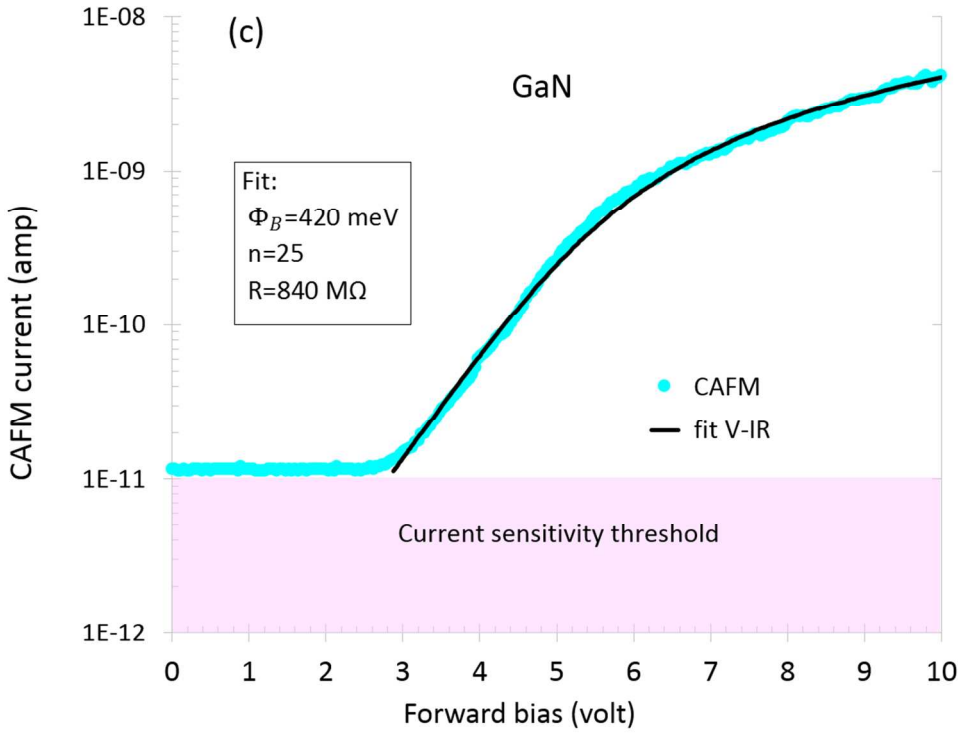

Figure S6. Current spectroscopy of the tip/MoS_2/GaN and tip/GaN structures with fitting using the equation (1).

The current-voltage curves for the point CAFM measurements on both MoS_2 and bare GaN substrate display rectifying behavior (Figure S6a) suggesting that interfaces, not the bulk, are dominant contributors to the resistance. The similar current range and the shape of the MoS_2 and GaN curves and the expectation of the nGaN/n^+GaN contact to be close to ohmic suggest that the I-V behavior is mostly set by the non-ohmic contact between the CAFM tip and the sample. The I-V curves on MoS_2 locations display higher currents and narrower location-to-location variation than the I-V curves at the GaN locations. Since the I-V measurements on GaN might be affected by the nanoscale growth structures described earlier in this section and that are unresolved in the AFM images, we focus our analysis of the I-V spectroscopy on the data from MoS_2 monolayers and show the data from the bare GaN locations only for comparison.

In order to de-convolute the embedded information on the MoS_2/GaN interface we analyzed the I-V curves at forward bias as shown in Figure S6b,c. At low bias voltages the current stays at the instrumental threshold level (approximately 10pA). From the threshold to 0.5 nA the I-V follows the exponential rise that starts saturating above 1nA. The same trend is true for the I-V curves of GaN. The current injection from a CAFM tip to a MoS_2 multilayer has been successfully described by Giannazzo *et al.* with the model of thermionic emission over the Schottky barrier[15]:

$$I = A_{tip} A^* T^2 e^{-\frac{q\Phi_B}{kT}} e^{\frac{q(V-IR)}{nkT}}, \qquad (1)$$

where *V* is the applied bias between the tip and the sample, *R* is the resistance contributing to the voltage drop between the back contact to the sample and the tip-semiconductor interface, A_{tip} is the tip-sample contact area, $A^* = 4\pi q k^2 m_{eff}/h^3$ is the Richardson constant with m_{eff} - effective mass

for electrons, h - Planck constant, T=293 K - the ambient temperature, q - elementary charge, Φ_B - height of the Schottky barrier at the tip-semiconductor interface measured from the Fermi level in the tip, k - Boltzmann constant, n - the ideality factor. We employed the formula (1) to fit all the I-V curves for MoS_2 and GaN with $A_{tip} \approx 100\ nm^2$[16] and the effective masses m_{eff} of $0.47\ m_e$ for monolayer MoS_2[17] and $0.20\ m_e$ for wurtzite GaN. Typical fitting results are displayed in Figure S6b,c. For the low currents (below 0.6 nA) the curves could be fit with a simple exponent described with two fitting parameters (Φ_B, n, R=0). At larger currents the I·R correction needed to be added to account for the discrepancy between the applied voltage and the voltage across the tip-semiconductor Schottky barrier. The extracted fitting parameters are Φ_B=370 meV, n=38, R=440 MΩ for MoS_2 and Φ_B=420 meV, n=25, R=840 MΩ for GaN. Large ideality factors raise a question on the applicability of the thermionic emission model for the tip-semiconductor contacts, suggesting that the extracted Schottky barrier heights need to be considered with caution. Nevertheless our value of Φ_B=370 meV for the barrier between monolayer MoS_2 and a doped diamond tip is not far from the reported Φ_B=307 meV for the multilayer MoS_2 and Pt-coated AFM tip[15]. The larger resistance R=840 MΩ for the GaN substrate is likely due to the smaller injection area in the top GaN and GaN/n^+GaN interface. The value of R=440 MΩ for MoS_2 includes the contact resistance of the MoS_2/GaN interface and is used in the main text to estimate the upper bound of the interface's contact resistivity.

Different types of AFM characterizations (topography, adhesion, and electrical surface potential) of the same MoS_2 triangle are displayed in Figure S7. The MoS_2 triangle exhibits higher adhesion to the CAFM tip than GaN. The presence of nano-dots (discussed in the main text as topographic spikes) is clearly visible in the topography and adhesion images at the perimeter of the triangle. The nano-dots are isolated and 3 to 5 nm in height and not to be confused with the sub-monolayer nanoscale growth contributing to the enhanced conductivity of the tip on GaN that is mentioned earlier in this section. The nano-dots are scattered over the GaN surface and have high density at the edges of the triangle. It is likely that the nano-dots are the re-deposition of MoO_x. The accumulation of the nano-dots near the edges might be due to the higher density of defect-related nucleation centers there.

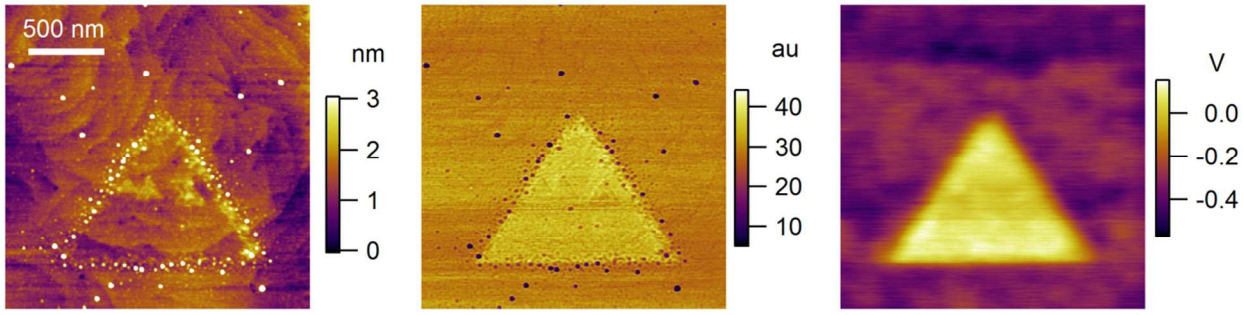

Figure S7. Topography, adhesion, and surface potential map of a MoS_2 triangle with some bilayer and trilayer growth.

4. X-ray photoelectron spectroscopy analysis

We measured three unique spots on MoS_2 /GaN in order to investigate how the material composition changes with the density of the MoS_2 structures (Figure S8). Concentration of Mo and S atoms (from Mo 3d and S 2s) increase in unison as measured from the downstream end of the wafer toward the upstream region (with respect to gas flow in the CVD furnace). This indicates that the MoS_2 concentration is higher for regions of the wafer closer to the precursor source. We observed the same trend with SEM measurements, where regions of the wafer close to the CVD source crucible show higher MoS_2 coverage. The ratio of MoO_x to MoS_2 decreases toward the upstream end of the wafer, as shown in Figure S8a. As the MoS_2 domains grow larger, the contribution of the MoO_x to the total Mo 3d signal diminishes. This is in accord with the picture where MoO_x redeposition is happening mostly on the bare GaN substrate. Also, this agrees with MoO_x nature of the nano-dots shown in Figure S7 since the density of the nano-dots is lower inside the MoS_2 structures. The deconvoluted O 1s spectra are shown in Figure S8e. We ascribe the low binding energy O 1s component (530.8 eV) to MoO_x, similar to previous measurements of Mo oxides[18]. The higher binding energy peak (532 eV) is related to oxidized surface carbon, since this peak tracks in intensity with the C 1s peak at 285.2 eV in Figure S8d.

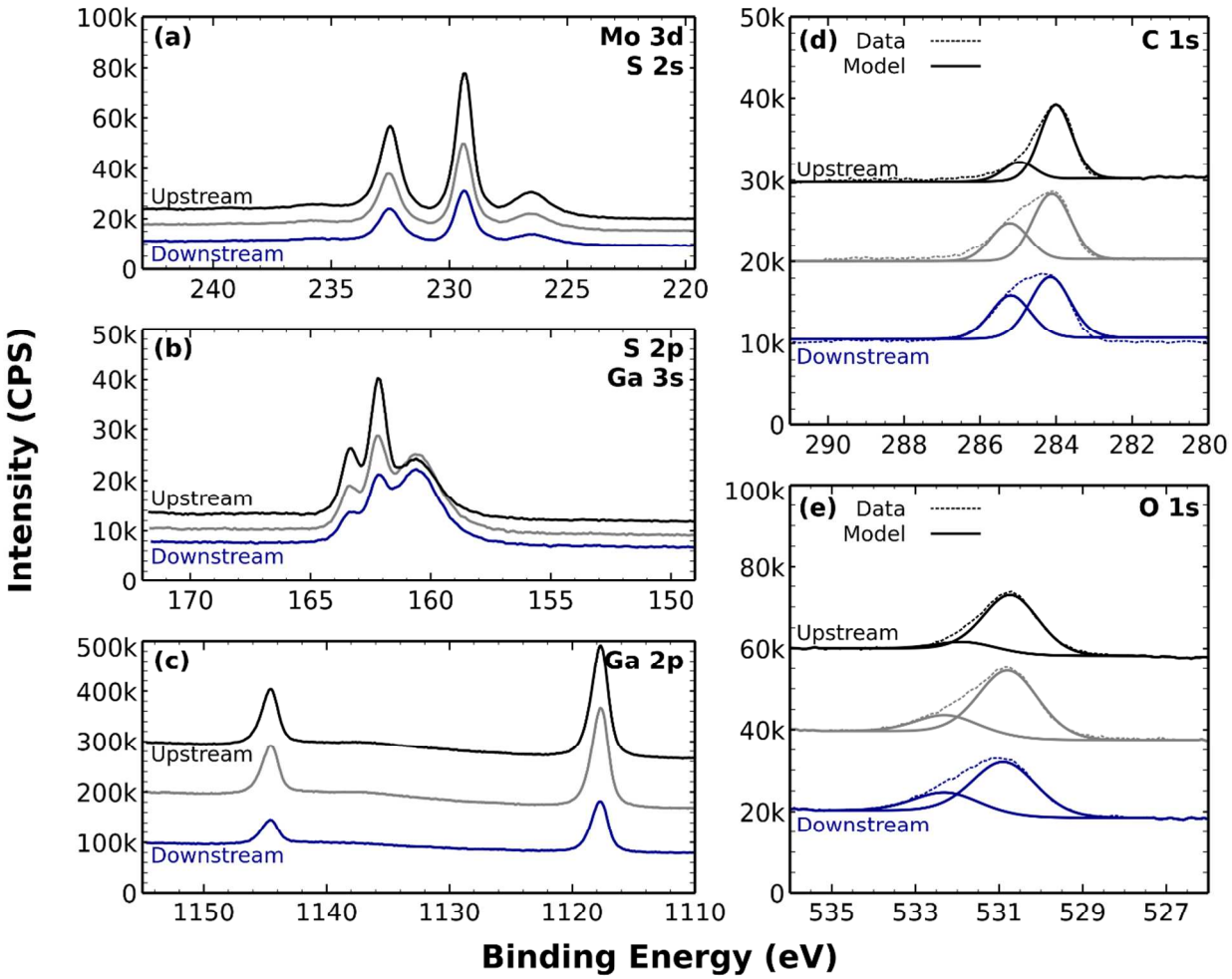

Figure S8. Comparison of Mo 3d, S 2s, S 2p, Ga 3s, Ga 2p, C 1s, and O 1s regions for upstream and downstream spots on the MoS_2/GaN/n-GaN/Sapphire stack.

As discussed in the main text, we evaluated the stability of GaN during CVD processing using a special CVD run. We ran a GaN/GaN/Sapphire wafer through the CVD process without loading the MoO_3 precursor. We compared this wafer to unprocessed GaN and to MoS_2/GaN. We first calculated the modified Auger parameters (α') for O 1s,KLL and Ga 3d,$L_3M_{45}M_{45}$ for each condition (Table S3), where the parameter is defined as the sum of the Auger transition kinetic energy and the core level peak binding energy. The parameter is a means of comparing the chemical state of a specific component, independent of differential charging effects.

Table S3. Auger parameter (A.P.) for oxygen and gallium from GaN, GaN+S, and GaN+MoS_2 surfaces.

Surface	O A.P.-1s,KLL (eV)	Ga A.P.-3d,$L_3M_{45}M_{45}$ (eV)
GaN	1042.5±0.2	1084±0.01
GaN + S	1042.8±0.2	1084.1±0
GaN + MoS_2	1042.3±0.2	1084.1±0.01

For oxygen, α' varies from 1042.3 to 1042.8 eV, which suggest that oxygen is primarily found in hydrocarbon form. Evidence for oxidized gallium is notably absent both in terms of Auger parameter values (α' for O 1s of Ga_2O_3 is expected to be 1041.4 eV[19]) and in the Ga core levels. Likewise, Ga α' values are consistent with GaN[19,20]. Since the MoS_2 overlayer is thin enough to be transparent to Ga photoelectrons, the lack of evidence for Ga_2O_3 indicates that the MoS_2/GaN interface is not oxidized during CVD. It is possible that the oxygen from the MoO_3 precursor is converted entirely into volatile SO_2 as a by-product of the MoS_2 growth[21]. On the other hand, the GaN surface subjected to a sulfur atmosphere at 800°C shows a small degree of sulfurization (1.3±0.1 atomic%, Table S4). A weak S 2s peak is detectable at 226.4 eV. Since the Auger parameters for GaN and gallium chalcogenides are very close, the exact assignment of this sulfur peak is difficult. Furthermore, the Ga 3s peak (Figure S9) completely obscures small S 2p doublets that may be expected in this region. Therefore, we cannot readily determine the identity of the S species on the surface.

Table S4. Atomic compositions measured by XPS for unprocessed (GaN), sulfur-exposed (GaN + S), and MoS_2-coated (GaN + MoS_2) GaN/GaN/Sapphire surfaces. Percentages are calculated using C 1s, Ga 3p, N 1s, O 1s, Mo 3d, and S 2s peaks. Each percentage is an average of three measurements.

	%C	%Ga	%N	%O	%Mo	%S
GaN	9.2 ± 0.6	44.8 ± 0.7	39.2 ± 0.4	6.8 ± 0.5	0 ± 0	0 ± 0
GaN + S	13.3 ± 0.6	41.9 ± 0.2	34.2 ± 0.4	9.2 ± 0.2	0 ± 0	1.3 ± 0.1
GaN + MoS_2	12.6 ± 1.5	34.1 ± 2.4	29.1 ± 2.8	8.8 ± 0.6	5.1 ± 2.5	10.3 ± 4.6

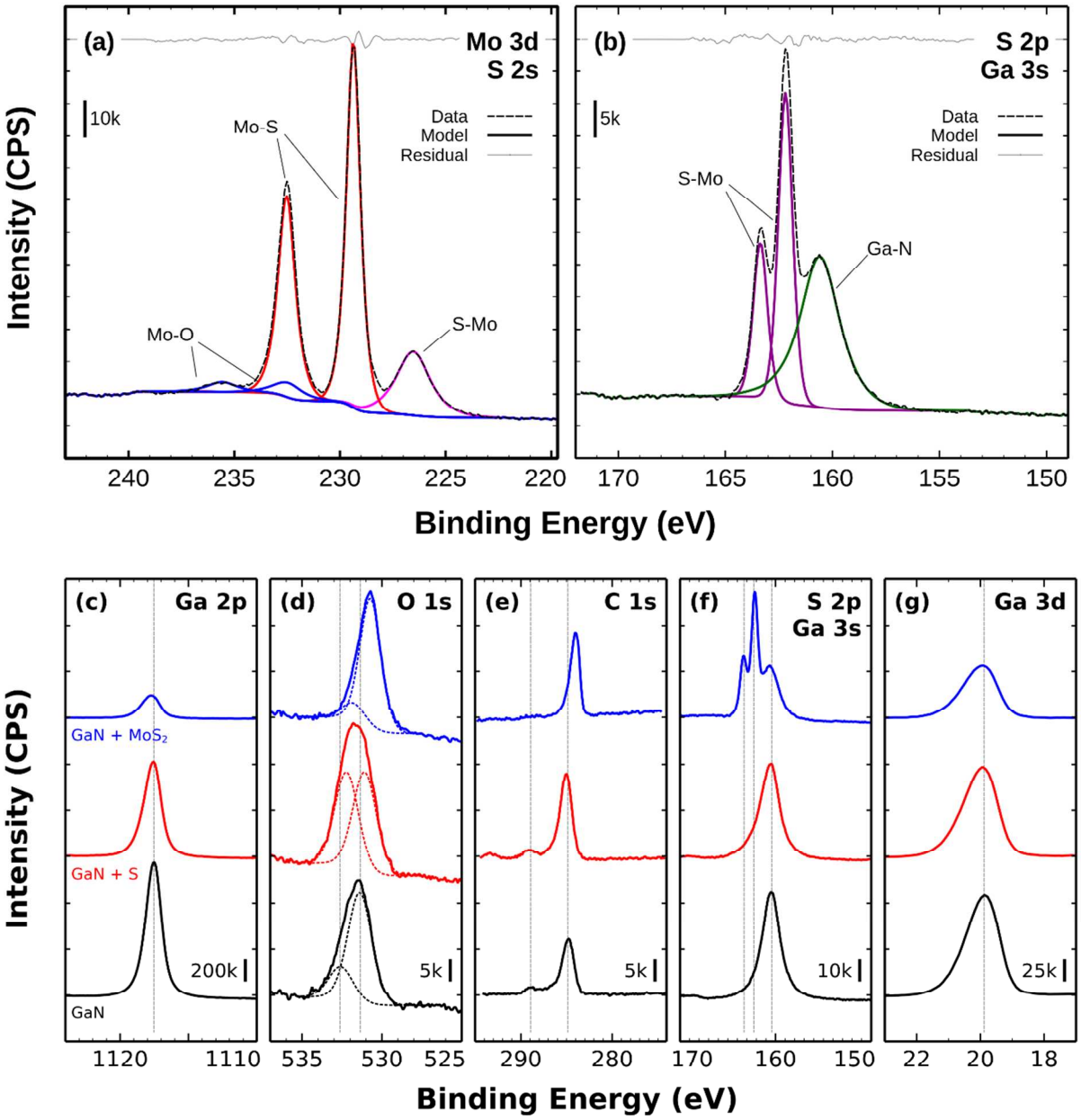

Figure S9. Core level spectra from (a) Mo 3d and (b) S 2p regions of MoS_2 on GaN. Panel (a) shows components from S 2s (MoS_2), Mo $3d_{5/2}$ and $3d_{3/2}$ doublets (MoS_2 and MoO_x). In (b), the S 2p doublet (MoS_2) and Ga 3s (GaN) are shown. Panels (c), (d), (e), (f), and (g) show a comparison of Ga 2p, O 1s, C 1s, S 2p, Ga 3s, and Ga 3d regions for the unprocessed GaN surface (bottom traces, black), GaN exposed to sulfur (middle traces, red), and GaN+MoS_2 (top traces, blue).

References

1. Lee, C.; Yan, H.; Brus, L. E.; Heinz, T. F.; Hone, J.; Ryu, S. Anomalous Lattice Vibrations of Single-and Few-Layer MoS2. *ACS Nano* **2010**, *4*, 2695–2700.
2. Li, H.; Zhang, Q.; Yap, C. C. R.; Tay, B. K.; Edwin, T. H. T.; Olivier, A.; Baillargeat, D. From Bulk to Monolayer MoS2: Evolution of Raman Scattering. *Adv. Funct. Mater.* **2012**, *22*, 1385–1390.

3. Molina-Sanchez, A.; Wirtz, L. Phonons in Single-Layer and Few-Layer MoS2 and WS2. *Phys. Rev. B* **2011**, *84*, 155413.
4. Lanzillo, N. A.; Birdwell, A. G.; Amani, M.; Crowne, F. J.; Shah, P. B.; Najmaei, S.; Liu, Z.; Ajayan, P. M.; Lou, J.; Dubey, M.; Nayak, Saroj K.; O'Regan, Terrance P. Temperature-Dependent Phonon Shifts in Monolayer MoS2. *Appl. Phys. Lett.* **2013**, *103*, 093102.
5. Rice, C.; Young, R. J.; Zan, R.; Bangert, U.; Wolverson, D.; Georgiou, T.; Jalil, R.; Novoselov, K. S. Raman-Scattering Measurements and First-Principles Calculations of Strain-Induced Phonon Shifts in Monolayer MoS2. *Phys. Rev. B* **2013**, *87*, 081307.
6. Chakraborty, B.; Bera, A.; Muthu, D. V. S.; Bhowmick, S.; Waghmare, U. V.; Sood, A. K. Symmetry-Dependent Phonon Renormalization in Monolayer MoS2 Transistor. *Phys. Rev. B* **2012**, *85*, 161403.
7. Zhou, K.-G.; Withers, F.; Cao, Y.; Hu, S.; Yu, G.; Casiraghi, C. Raman Modes of MoS2 Used as Fingerprint of van Der Waals Interactions in 2-D Crystal-Based Heterostructures. *ACS Nano* **2014**, *8*, 9914–9924.
8. Splendiani, A.; Sun, L.; Zhang, Y.; Li, T.; Kim, J.; Chim, C.-Y.; Galli, G.; Wang, F. Emerging Photoluminescence in Monolayer MoS2. *Nano Lett.* **2010**, *10*, 1271–1275.
9. Mak, K. F.; Lee, C.; Hone, J.; Shan, J.; Heinz, T. F. Atomically Thin MoS2: A New Direct-Gap Semiconductor. *Phys. Rev. Lett.* **2010**, *105*, 136805.
10. Chernikov, A.; Berkelbach, T. C.; Hill, H. M.; Rigosi, A.; Li, Y.; Aslan, O. B.; Reichman, D. R.; Hybertsen, M. S.; Heinz, T. F. Exciton Binding Energy and Nonhydrogenic Rydberg Series in Monolayer WS2. *Phys. Rev. Lett.* **2014**, *113*, 076802.
11. Ugeda, M. M.; Bradley, A. J.; Shi, S.-F.; Felipe, H.; Zhang, Y.; Qiu, D. Y.; Ruan, W.; Mo, S.-K.; Hussain, Z.; Shen, Z.-X.; Wang, Feng; Louie, Steven G.; Crommie, Michael F. Giant Bandgap Renormalization and Excitonic Effects in a Monolayer Transition Metal Dichalcogenide Semiconductor. *Nat. Mater.* **2014**.
12. Li, W.; Birdwell, A. G.; Amani, M.; Burke, R. A.; Ling, X.; Lee, Y.-H.; Liang, X.; Peng, L.; Richter, C. A.; Kong, J.; Gundlach, David J.; Nguyen, N. V. Broadband Optical Properties of Large-Area Monolayer CVD Molybdenum Disulfide. *Phys. Rev. B* **2014**, *90*, 195434.
13. Li, Y.; Qi, Z.; Liu, M.; Wang, Y.; Cheng, X.; Zhang, G.; Sheng, L. Photoluminescence of Monolayer MoS2 on LaAlO3 and SrTiO3 Substrates. *Nanoscale* **2014**, *6*, 15248–15254.
14. Su, W.; Dou, H.; Li, J.; Huo, D.; Dai, N.; Yang, L. Tuning Photoluminescence of Single-Layer MoS2 Using H2O2. *RSC Adv* **2015**, *5*, 82924–82929.
15. Giannazzo, F.; Fisichella, G.; Piazza, A.; Agnello, S.; Roccaforte, F. Nanoscale Inhomogeneity of the Schottky Barrier and Resistivity in MoS2 Multilayers. *Phys. Rev. B* **2015**, *92*, 081307.
16. Yao, N.; Wang, Z. L. *Handbook of Microscopy for Nanotechnology*; Springer, 2005.
17. Yu, S.; Xiong, H. D.; Eshun, K.; Yuan, H.; Li, Q. Phase Transition, Effective Mass and Carrier Mobility of MoS2 Monolayer under Tensile Strain. *Appl. Surf. Sci.* **2015**, *325*, 27–32.
18. Leung, Y. L.; Wong, P. C.; Zhou, M. Y.; Mitchell, K. A. R.; Smith, K. J. XPS Studies of the Nitridation of MoO3 Thin Films on Alumina and Silica Supports. *Appl. Surf. Sci.* **1998**, *136*, 178–188.
19. NIST X-Ray Photoelectron Spectroscopy Database, Version 4.1 (National Institute of Standards and Technology, Gaithersburg); Http://srdata.nist.gov/xps/, **2012**.
20. Perry, D. L. Application of Combined X-Ray Photoelectron/Auger Spectroscopy to Studies of Inorganic Materials. In *Applications of Analytical Techniques to the Characterization of Materials*; Perry, D. L., Ed.; Springer US, 1991; pp. 1–23.
21. Senthilkumar, V.; Tam, L. C.; Kim, Y. S.; Sim, Y.; Seong, M.-J.; Jang, J. I. Direct Vapor Phase Growth Process and Robust Photoluminescence Properties of Large Area MoS2 Layers. *Nano Res.* **2014**, *7*, 1759–1768.